FINAL REPORT

# ANALYSIS OF NOAA--MSFC GOES X-RAY TELESCOPE

David L. Shealy, Ph.D.
Bardon Environmental Consultants, Inc.
713 Comer Drive
Birmingham, AL 35216

Submitted to George C. Marshall Space Flight Center, Alabama 35812, July 31, 1979, under purchase order no. H-34373B.



TABLE OF CONTENTS



List of Figures

List of Tables

## I. Introduction

The purpose of this study is to perform the following tasks:

TASK A: Verify the basic mirror design parameters and performance assessments of the NOAA-MSFC GOES x-ray telescope as provided to the principal investigator by MSFC technical personnel.

TASK B: Perform computer ray trace analysis to establish spot size and point response function on-axis and off-axis at 5,10,16, and 20 arc-minutes by plotting the line spread function.

TASK C: Determine resolution improvements and efficiency losses by shortening the hyperboloid length of the telescope to introduce intentional vignetting.

TASK D: Generate a computer magnetic tape of the mirror radius as a function of position along the optical axis to be used in the mirror diamond turning activity.

The general telescope system was assumed to be a paraboloid-hyperboloid in a Wolter Type 1 configuration. A brief discussion is given in section II of the equations which specify the telescope parameters and the resolution as a function of the collecting area using the empirical formulas of Van-Spreybroech and Chase.[1] Section III contains a discussion of the computer ray trace code used to determine the spot size and point response function for off-axis rays. In section IV, the measured resolution of the Goddard ATM x-ray telescope (S-056) is compared to the rms blur circle radius and the full width half maximum of the line spread function. An empirical scaling formula, Eq. 26, which transforms the rms blur circle radius into a more accurate measure of resolution, is introduced. The geometrical imaging properties of the proposed NOAA-MSFC GOES x-ray telescope are discussed in section V. The conclusions of this study are presented in section VI. Appendix A contains a discussion of alternate mirror designs for the NOAA-MSFC GOES x-ray telescope.

## II. Defining and Analysis Equations of a WOLTER type I X-ray Telescope

In this section a brief discussion will be given of the equations that specify the mirror surface parameters of a WOLTER 1 x-ray telescope and the resolution of the telescope as a function of the collecting area. The notation is that of Mangus and Underwood.[2]

The defining equations of the paraboloid (P) and hyperboloid (H) surfaces are given by

$$y_p^2 = p(2x_p + p) \tag{1a}$$

$$\frac{(x_H - c)^2}{a^2} - \frac{y_H^2}{b^2} = 1 \tag{1b}$$

where the coordinate system is defined in Fig. 1. The constants a, b, c, and p are determined by requiring the paraboloid and hyperboloid to be confocal (see Fig. 1) and the glancing angle on both the P and H mirror to be $\theta_m$ at the intersection point of the mirrors. Explicitly, require the slope of P at intersection point $(x_{p,min}, y_{p,min})$ to be $\tan\theta_m$

$$\frac{dy_{p,min}}{dx_{p,min}} = \frac{p}{y_{p,min}} = \tan\theta_m$$

or

$$p = y_{p,min} \tan\theta_m \tag{2}$$

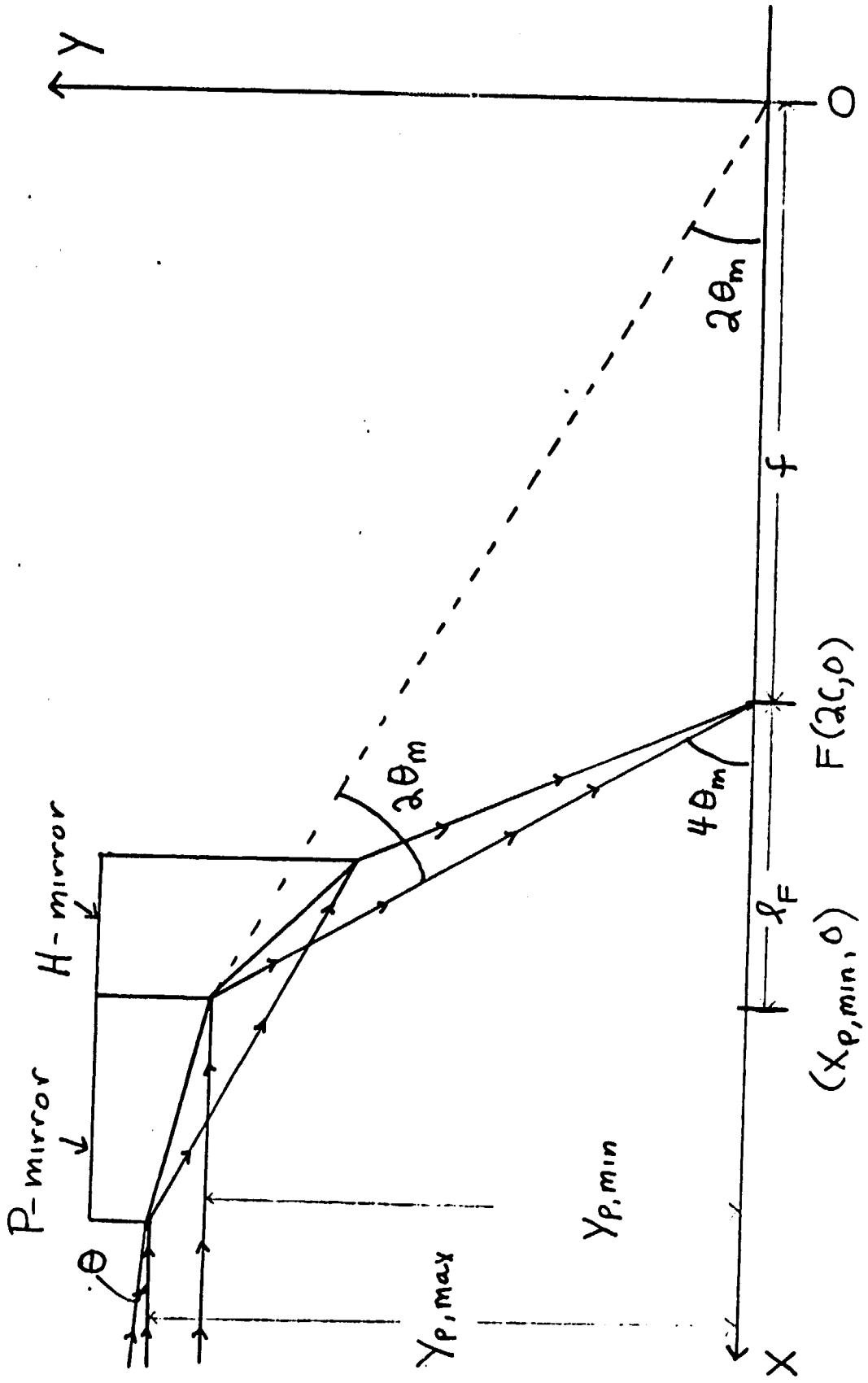
Y
O
$2\theta_m$
f
$2\theta_m$
$4\theta_m$
F(2C,0)
H-mirror
P-mirror
$\theta$
$y_{p,max}$
$y_{p,min}$
$\ell_F$
$(x_{p,min},0)$
X

FIGURE 1

If we define the focal length, f, of the telescope as the distance along the ray from the intersection point of P and H mirrors to the focal point, then

$$y_{p,min} = f \sin(4\theta_m) = y_{H,max} \tag{3}$$

where it has been assumed that the slope of H at the intersection point is tan $3\theta_m$ and glancing angle of ray on H at the intersection point is $\theta_m$ such that the ray will make angle $4\theta_m$ with the optical axis. Evaluating $x_{p,min}$ from (1a) and using (3) gives

$$x_{p,min} = 2f \cos^2(2\theta_m) \tag{4}$$

Note further that if the ray reflected from P at intersection is extended to the origin, this virtual ray will make an angle $2\theta_m$ with both the optical axis and the actual ray reflected from H at intersection to the focal point. Hence

$$f = \overline{OF} = 2C \tag{5}$$

where the last equality follows since $\overline{OF}$ is the distance between the two foci of the hyperboloid. One also knows from the general properties of

a hyperboloid

$$a^2 + b^2 = c^2 \tag{6}$$

Hence, it remains to relate the constant a to f and $\Theta_m$ in order to define completely the P and H mirror parameters.

Since $x_{H,max} = x_{p,min}$ and $y_{p,min} = y_{p,max}$ at the intersection point of the P and H mirrors, then Eq. 1b at the intersection point can be rewritten as

$$\frac{[2f\cos^2(2\theta_m) - c]^2}{a^2} - \frac{f^2\sin^2(4\theta_m)}{b^2} = 1 \tag{7}$$

where Eqs. 3 and 4 have been used. Equation 7 may be rewritten as

$$\frac{f^2}{4}\frac{[4\cos(2\theta_m)-1]^2}{a^2} - \frac{f^2\sin^2(4\theta_m)}{\frac{f^2}{4} - a^2} = 1 \tag{7a}$$

where Eqs 5-6 have been used. If the constant a is given by

$$a = \frac{f}{2}[2\cos(2\theta_m)-1] \tag{8}$$

then equation 7a is satisfied. The P and H mirror are given by

$$\begin{aligned} \rho &= y_{p,min}\tan\theta_m \\ a &= \frac{f}{2}[2\cos(2\theta_m)-1] \\ b^2 &= c^2 - a^2 \\ c &= f/2 \end{aligned} \tag{9}$$

and the focal length is defined by

$$f\sin(4\theta_m) = y_{p,min} = y_{H,max} \tag{10}$$

Referring th Fig. 1 it is clear that the axial length from the intersection of the P-H mirrors to the focal point is

$$\begin{aligned} \ell_F &\equiv x_{p,min} - f \\ &= f\left[2\cos^2(2\theta_m) - 1\right] \end{aligned} \tag{11}$$

where Eq. 4 has been used.

The collecting area for axial rays incident upon the telescope is defined by

$$A = \pi\left(y_{p,max}^2 - y_{p,min}^2\right) \tag{12}$$

In the present application a specific value for $y_{p,max}$ is determined by requiring the total length of the telescope, $\ell_T$, to be given. That is,

$$\begin{aligned} x_{p,max} &= \ell_T + f \\ y_{p,max} &= \left[-p\left(2x_{p,max} + p\right)\right]^{1/2} \end{aligned} \tag{13}$$

Also, the axial length of the P mirror is given by

$$\ell_p = \ell_T - \ell_F \tag{14}$$

The length of the H mirror is determined by

$$\ell_H = x_{H,max} - x_{H,min} \tag{15}$$

where $x_{H,min}$ is evaluated from the ray trace by evaluating where the ray which is reflected from $(x_{p,max}, x_{p,max})$ intersects the H mirror. The ray

trace code is discussed in section III.

The empirical formulas of VanSpeybroech and Chase for the rms blur circle radius, $\sigma_D$, are useful for evaluating alternative mirror designs. However, it is desirable to express $\sigma_D$ explicitly in terms of the collecting area A. From Eq. 4 of Ref. 1, $\sigma_D$ for a flat image surface is given by

$$\sigma_D = \frac{1}{20\pi} \frac{\tan^2\theta}{\tan^3\theta_m} \frac{A}{\ell_F^2} + 4 \tan\theta \tan^2\theta_m \qquad (16)$$

where $\theta$ is the off-axis field angle and $\sigma_D$ is measured in radians. The collecting area is approximately given by

$$A = 2\pi y_{p,min} \ell_p \tan\theta_m \qquad (17a)$$

or

$$A = 2\pi f \sin(4\theta_m) \tan\theta_m [\ell_T - \ell_F] \qquad (17b)$$

By comparing Eqs 16-17 , it is clear that Eq. 16 is not an explicit function of A, since A depends on $\ell_F$ in Eq. 17b. In order to plot $\sigma_D$ versus A, it is necessary to obtain an expression for $\ell_F$ in terms of $\ell_T$, A, and $\theta_m$. From Eq. 17a we have

$$\ell_p = \frac{A}{2\pi y_{p,min} \tan\theta_m} \qquad (18)$$

Eliminating $\ell_p$ between Eq. 14 and 18 gives

$$\ell_T = f[2\cos^2(2\theta_m) - 1] + \frac{A}{2\pi f \tan\theta_m \sin(4\theta_m)} \qquad (19)$$

which may be rearranged into a quadratic equation for the focal length f :

$$f^2[2\cos^2(2\theta_m)-1] - \ell_T f + \frac{A}{2\pi \tan\theta_m \sin(4\theta_m)} = 0 \qquad (20)$$

which has the solutions

$$f = \frac{\ell_T \pm \left\{\ell_T^2 - \frac{4A[2\cos^2(2\theta_m)-1]}{2\pi \tan\theta_m \sin(4\theta_m)}\right\}^{1/2}}{2[2\cos^2(2\theta_m)-1]} \qquad (21)$$

The "+" sign in Eq. 21 corresponds to the physically valid solution. Therefore, $\ell_F$ is given by

$$\ell_F = \frac{\ell_T}{2} + \frac{1}{2}\left\{\ell_T^2 - \frac{2A[2\cos^2(2\theta_m)-1]}{\pi \tan\theta_m \sin(4\theta_m)}\right\}^{1/2} \qquad (22)$$

Equation 22 represents the desired expression for $\ell_F$ expressed in terms of $\ell_T$, A, and $\theta_m$. Using Eq. 22, $\sigma_D$ may be evaluated from Eq. 16. Further discussion of Eqs. 16 and 22 will be given in Appendix A.

## III. Ray Trace Code

In this section, a brief discussion of the ray trace code used in this study is given. A detailed discussion of the ray trace equations as applied to a Wolter Type 1 x-ray telescope has been given by Forman, et. al.[3] The computer ray trace program can be broken down into the following parts:

1.a. Define input constants : $a,b,c,p,y_{p,min},y_{p,max},x_{p,max}, \ell_H, \theta_m$.

b. Assign directions cosines to an incident ray. It has been assumed that the incident ray is in the x-y plane and makes an angle $\theta$ with respect to the x axis. The angle $\theta$ assumed values 0,1,2..., 20 arc-mins.

c. Set up a grid on the entrance pupil, which is an imaginary plane perpendicular to the optical axis located at $x_{p,max}$, such that each ray will pass through equal areas on the entrance pupil. For example, the polar coordinates R, $\phi$ on the entrance pupil are given by

$$\phi = 0, \Delta\phi, 2\Delta\phi, \cdots, 360-\Delta\phi$$

where $\Delta\phi$ = 360/(NPHO-1). The radial coordinates are given by

$$R = R_1 (= y_{p,min}), R_2 (= \sqrt{R_1^2+\Delta}), \cdots$$
$$\cdots, R_{NRO} (= \sqrt{R_1^2 + (NRO-1)\Delta} = y_{p,max})$$

where $\Delta = (y_{p,max}^2 - y_{p,min}^2)/(NRO - 1)$. When evaluating the rms blur circle radius from the ray trace data, it is sufficient to take NPHO = 140 and NRO = 30 for a total of 4,200 rays to be traced through the telescope at normal incidence. However, when the point spread function is being evaluated from the ray trace data, a total of 300,000 rays were traced through the x-ray telescope. As a result of the large number of rays traced for the point spread function, the angular variable $\phi$ in the entrance pupil only assumed values from 0 to 180° with NPHO = 3,000 and NRO = 50. The symmetry of the telescope about the x-y plane is used to obtain the intercepts of the rays which would have passed through the entrance pupil for $\phi$ = 180° to 360°.

2. For each field angle $\Theta$, separate rays are traced through each grid point $(R, \phi)$ on the entrance pupil. The intercept $(x_p, y_p)$ on the P mirror is evaluated. It is confirmed that the point $(x_p, y_p)$ is on the physical P mirror surface of length $\ell_p$. A vector form of Snell's law is used to determine the direction cosines of the reflected ray from the P mirror. The intercept $(x_H, y_H)$ with the H mirror is computed and Snell's law for reflection is applied to evaluate the direction cosines of the ray reflected from the H mirror into the image space. The ray is accepted by the telescope if the point $(x_H, y_H)$ is on the physical H mirror surface of length $\ell_H$. The The ray intercept with the Gaussian image plane is also computed. The various summations required in the rms blur circle calculations[4] are also evaluated.

3. After completing the ray trace for all grid points at a given field angle, the rms blur circle radius is evaluated for a series of image planes by using the formulas of Ref. 4. Also, the location of the optimum image surface, ie, loci of image points with minimum rms blur circle radius, is also computed.

4. The point response function is evaluated by setting up a 40 x 40 uniform grid on the image surface. For each field angle, the ray intercepts with the image plane are sorted into different image grid locations. The result is a distribution of rays over the image grid cells. The number of rays per image plane cell time the element of area $\Delta A$ (= collecting area/total number of rays incident upon the telescope) is a measure of the point response function.

## IV. Measured Resolution of the S-056 X-ray Telescope

It has been observed by Werner[5] that the full width half maximum (FWHM) of the line spread function (LSF) is a more accurate measure of the observed resolution of an x-ray telescope than the rms blur circle radius. The experimental results which support this conclusion have been known for a number of years, but have not been generally recognized. It follows from the point response function for S-056 x-ray telescope[3] that the FWHM is approximately equal to 1 arc-sec at a field angle of 16 arc-min. However, from Fig. 2 the rms blur circle radius for S-056 as computed by the empirical formulas of VanSpeybroech and Chase, Eq. 16, is 8 arc-sec at a field angle of 16 arc-min. Whereas, the actual, measured resolution of the S-056 telescope for visible light is given by the X's in Fig. 3. It follows by comparing Figs. 2 and 3 that the rms blur circle radius does not provide a reasonable measure of the resolution of an x-ray telescope.

Since the rms blur circle radius is easier to evaluate than the point response function from ray trace data, it is desirable to establish a scaling technique between the rms blur circle radius and measured resolution. If one assumes the measured resolution, R, in arc-sec of an x-ray telescope is a linear function of the field angle, $\theta$, in arc-min which passes through the origin

$$R = \beta\theta \tag{23}$$

then, fitting the data of Fig. 3 in a least squared sense yields the constant

$$\beta = 8.5375 \times 10^{-2} \text{ arc-sec/arc-min.} \tag{23a}$$

It is desirable to evaluate a scaling function $a(\theta)$ which will transform the rms blur circle radius into a meaningful measure of resolution. Assume

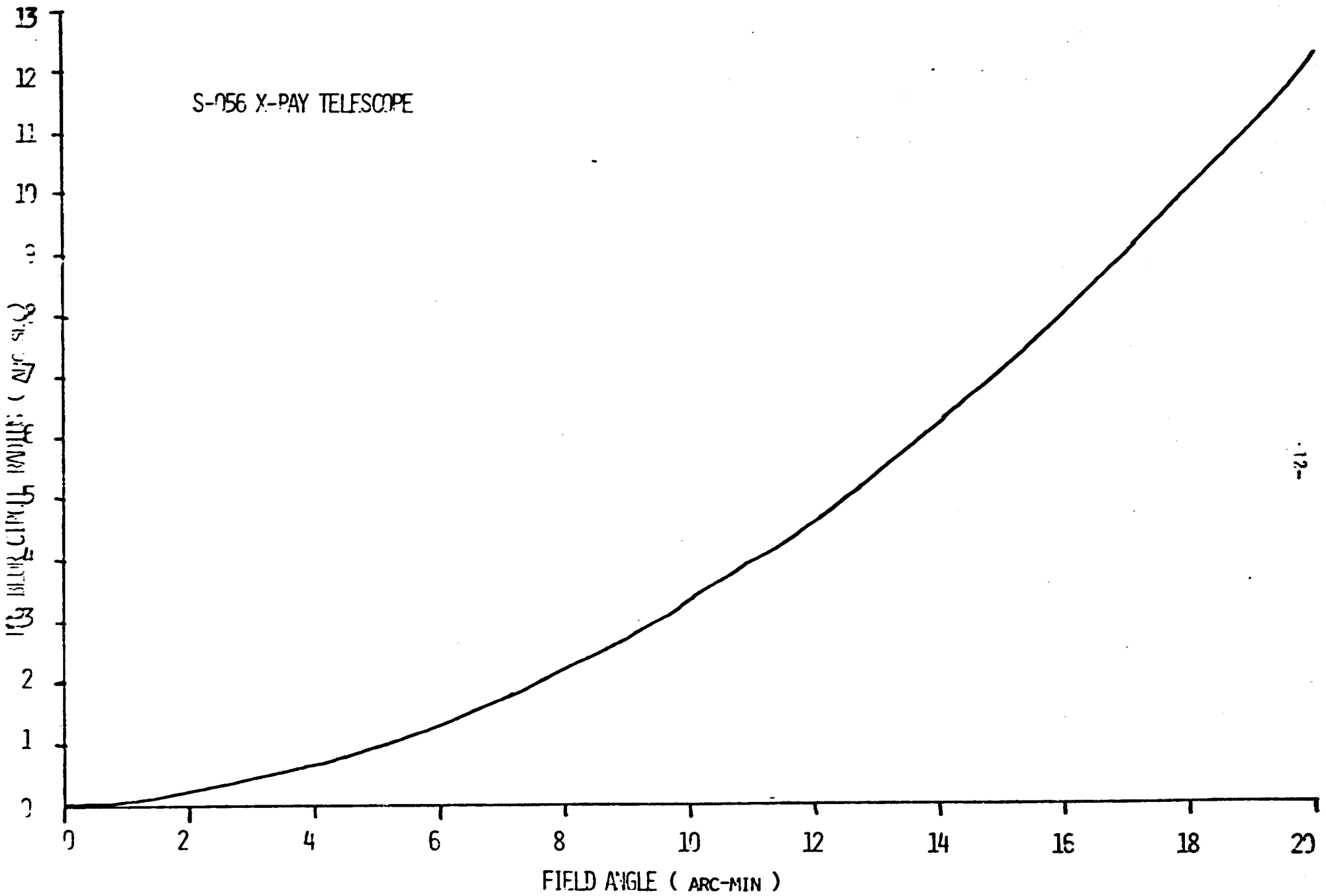
S-056 X-PAY TELESCOPE
13
12
11
10
9
8
7
6
5
4
3
2
1
0
0
2
4
6
8
10
12
14
16
18
20
FIELD ANGLE ( ARC-MIN )

Fig. 2

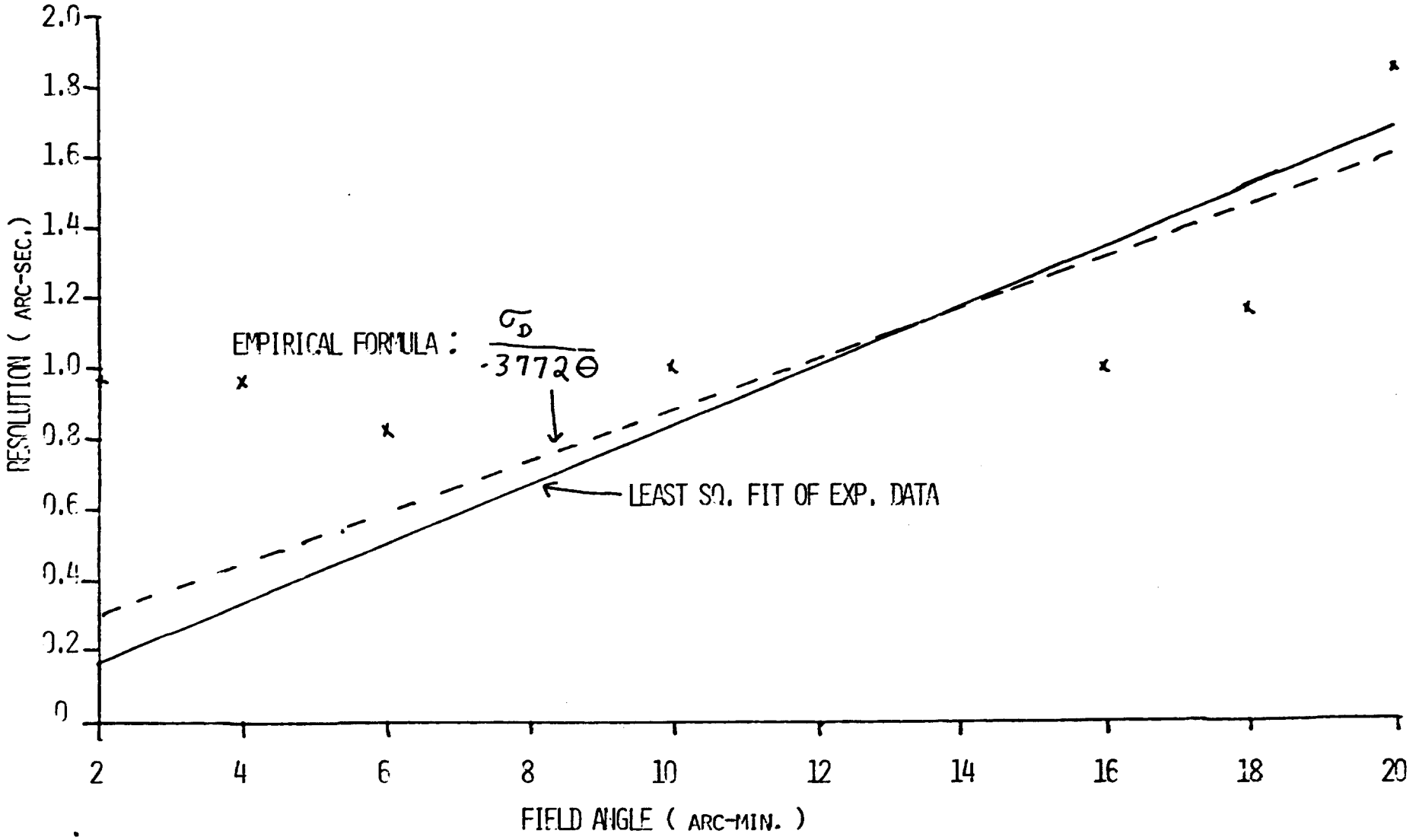
2.0
1.8
1.6
1.4
1.2
1.0
0.8
0.6
0.4
0.2
0
RESOLUTION ( ARC-SEC. )
EMPIRICAL FORMULA : $\frac{\sigma_D}{.3772\Theta}$
LEAST SQ. FIT OF EXP. DATA
2
4
6
8
10
12
14
16
18
20
FIELD ANGLE ( ARC-MIN. )

Fig. 3

$$R = a(\Theta)\sigma_D \tag{24}$$

The two simplest forms for $a(\Theta)$ are

$$a(\Theta) = \alpha\Theta \tag{24a}$$

$$a(\Theta) = 1/\gamma\Theta \tag{24b}$$

Evaluating $\alpha$ by requiring $\alpha\Theta$ fit the $(R/\sigma_D)$ data in column 4 of Table 1 in a least squared sense yields

$$\alpha = 0.015635/\text{ arc-min} \tag{25a}$$

Whereas, evaluating $\gamma$ by requiring $\gamma\Theta$ fit the $(\sigma_D/R)$ data in column 5 of Table 1 in a least squared sense yields

$$\gamma = 0.377207 / \text{ arc-min} \tag{25b}$$

Table 2 displays $\alpha\Theta\sigma_D$ and $(\sigma_D/\gamma\Theta)$ as a function of $\Theta$. By comparing columns 2 and 3 of Table 2 with column 2 of Table 1, it is clear that column 3 of Table 2 is a better fit to R. Hence, the empirical formula

$$R = \sigma_D / (0.377207\Theta) \tag{26}$$

yields a better estimate of the measured resolution of the S-056 x-ray telescope than the rms blur circle radius data. From Fig. 3, it is apparent that the empirical formula, Eq. 26, offers a reasonable measure of the resolution of an x-ray telescope. We shall assume Eq. 26 is valid in general for x-ray telescopes and will apply Eq. 26 to the GOES x-ray telescope to establish the resolution from the rms blur circle radius data. The point spread function for the GOES x-ray telescope is also evaluated in section V.

TABLE 1

| $\Theta$(arc-min) | $R = \beta\,\Theta$(arc-sec) | $\sigma_D$(arc-sec) | $\frac{R}{\sigma_D}$ | $\frac{\sigma_D}{R}$ |
|---|---|---|---|---|
| 2 | .16875 | .22884 | .737421 | 1.35647 |
| 4 | .33750 | .67844 | .49746 | 2.01020 |
| 6 | .50625 | 1.34882 | .37533 | 2.66434 |
| 8 | .6750 | 2.23996 | .301345 | 3.31846 |
| 10 | .84375 | 3.35188 | .25173 | 3.97259 |
| 12 | 1.0125 | 4.68457 | .21614 | 4.62674 |
| 14 | 1.18125 | 6.23804 | .18936 | 5.28089 |
| 16 | 1.350 | 8.01229 | .16849 | 5.93504 |
| 18 | 1.51875 | 10.00733 | .15176 | 6.58918 |
| 20 | 1.68750 | 12.22316 | .13806 | 7.24333 |

TABLE 2

| $\Theta$ (arc-min) | $\alpha\Theta\sigma_D$ (arc-sec) | $\sigma_D$ (arc sec) / $\gamma\Theta$ |
|---|---|---|
| 2 | .00716 | .30333 |
| 4 | .04243 | .44965 |
| 6 | .12653 | .59597 |
| 8 | .28017 | .74229 |
| 10 | .52407 | .88860 |
| 12 | .87892 | 1.03492 |
| 14 | 1.36544 | 1.18125 |
| 16 | 2.00435 | 1.32757 |
| 18 | 2.81642 | 1.47389 |
| 20 | 3.82218 | 1.62022 |

## V. Geometrical Imaging Properties of the NOAA-MSFC GOES X-Ray Telescope

Based on discussions with MSFC personnel, the mirror parameters were evaluated for a telescope defined by

$$f = 26\,\text{in.} = 66.04\,\text{cm.}$$
$$\theta_m = 130\,\text{arc-mins.} \qquad (27)$$
$$\ell_T = 30\,\text{ins} = 76.2\,\text{cm.}$$

From Eq. 9, the P-H mirror parameters were found to be

$$p = 0.37649195\,\text{cm.}$$
$$a = 32.8312\,14\,\text{cm.}$$
$$b = 3.525\,8707\,\text{cm.} \qquad (28a)$$
$$c = 33.02\,\text{cm.}$$

and from Eqs. 3-4,10-12

$$X_{p\text{-min}} = 131.325937\,\text{cm.}$$
$$Y_{p\text{-min}} = 9.951284\,\text{cm.} \qquad (24b)$$
$$X_{p,\,max} = 142.24\,\text{cm.}$$
$$Y_{p,\,max} = 10.355973\,\text{cm.}$$
$$A = 25.817966\,\text{cm.}^2$$
$$\Delta A = 8.60742 \times 10^{-5}\,\text{cm}^2/\text{ray}$$

The length of P-H mirrors and $\ell_F$ are given by:

$$\ell_p = 10.914063\,\text{cm.}$$
$$\ell_H = 9.308834\,\text{cm.} \qquad (28c)$$
$$\ell_F = 65.285937\,\text{cm.}$$

The mirror parameters given by Eqs. 28 a,b,c have been evaluated independently by the principal investigator and are in agreement with those obtained by MSFC personnel.

A computer ray trace analysis has been performed on the telescope defined by Eqs. 28 to determine the rms blur circle radius as a function of the field angle for different image plane locations. Figure 4 presents the rms blur circle radius vs. the field angle for 7 image plane locations. The label "$\Delta$ z" in Fig. 4 specifies the displacement of the image plane from the focal point towards the telescope in cm. From the curves presented in Fig. 4, it is clear that the depth of field is sharply defined and may present tight tolerances for positioning the image plane during assembly of the telescope. Figure 5 displays the resolution as predicted by the empirical formula, Eq. 26, for the GOES x-ray telescope. Based on these results, one may expect an actual resolution for the GOES x-ray telescope to be less than 2.5 arc-sec at a field angle of 20 arc-min. In order to confirm these results, the meridional (x-y plane) line spread function (LSF) and the sagittal LSF have been evaluated from the point spread function as computed from the ray trace data for field angles $\theta$ = 5,10,16,20 arc-min. The meridional LSF's are given in Figs. 6a,b,c,d for $\theta$ = 5,10,16,20 arc-min, respectively. The FWHM's of the LSF's given in Figs. 6a-d are displayed in Fig. 5 as the "$\Delta$" symbols. A straight line which approximates the FWHM of the meridional LSF has also been given. (The plate factor used to express the FWHM in angular units is $(180*360/\pi f)$ = 3,123.314 arc-sec/radian where f = 66.04 cm for GOES.) It may be concluded from Fig. 5 that the empirical formula, Eq. 26, and the FWHM of the meridional LSF agree reasonably well at large field angles and differ by a factor of 2 for small field angles. Whereas, the rms blur circle radius and the FWHM of the LSF differ by almost an order of magnitude.

The sagittal LSF's for a field angle of 5,10,16,20 arc-min are given in Figs. 7a,b,c,d. The FWHM's for Figs. 7a-d are plotted in Fig. 5 as the "+" symbols. From these results, Figures 5-7, it follows that the resolution of the GOES x-ray telescope should be less than 3 arc-sec at a field angle of

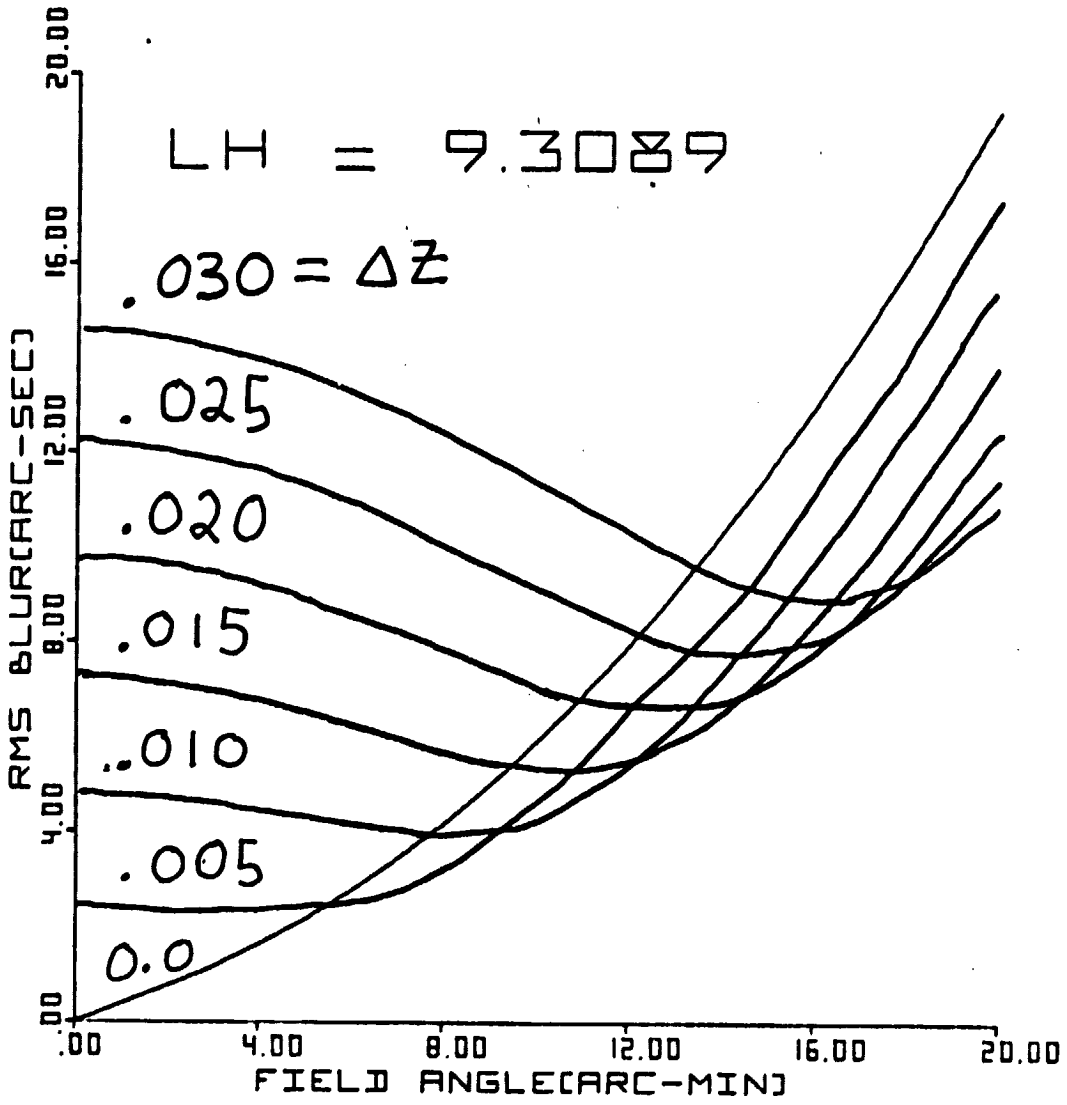
LH = 9.3089
.030 = ΔZ
.025
.020
.015
..010
.005
0.0
RMS BLUR(ARC-SEC)
20.00
16.00
12.00
8.00
4.00
.00
.00
4.00
8.00
12.00
16.00
20.00
FIELD ANGLE(ARC-MIN)

Fig. 4

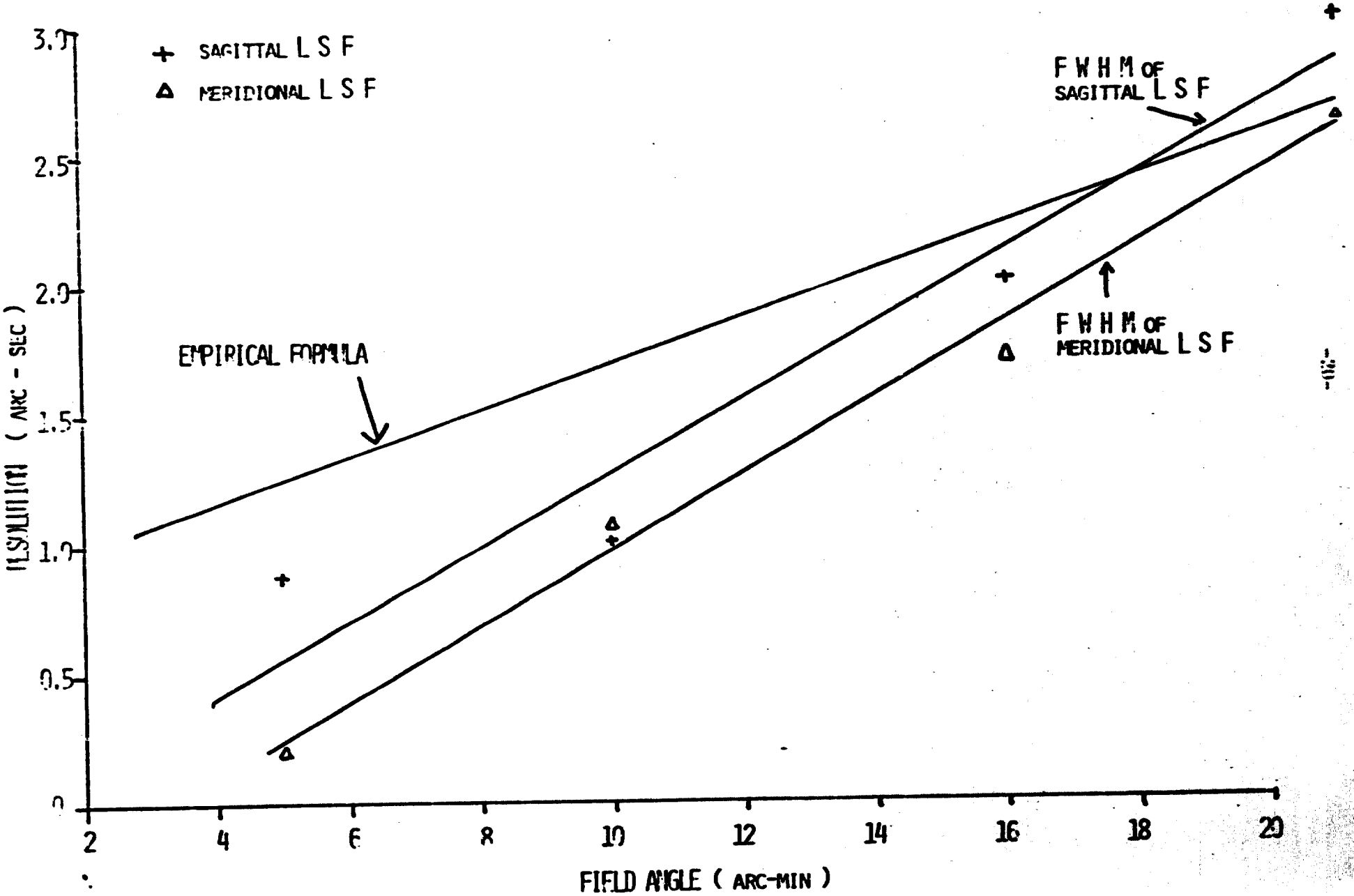
SAGITTAL L S F
MERIDIONAL L S F
FWHM OF SAGITTAL L S F
FWHM OF MERIDIONAL L S F
EMPIRICAL FORMULA
3.0
2.5
2.0
1.5
1.0
0.5
0
2
4
6
8
10
12
14
16
18
20
FIELD ANGLE ( ARC-MIN )

Fig. 5

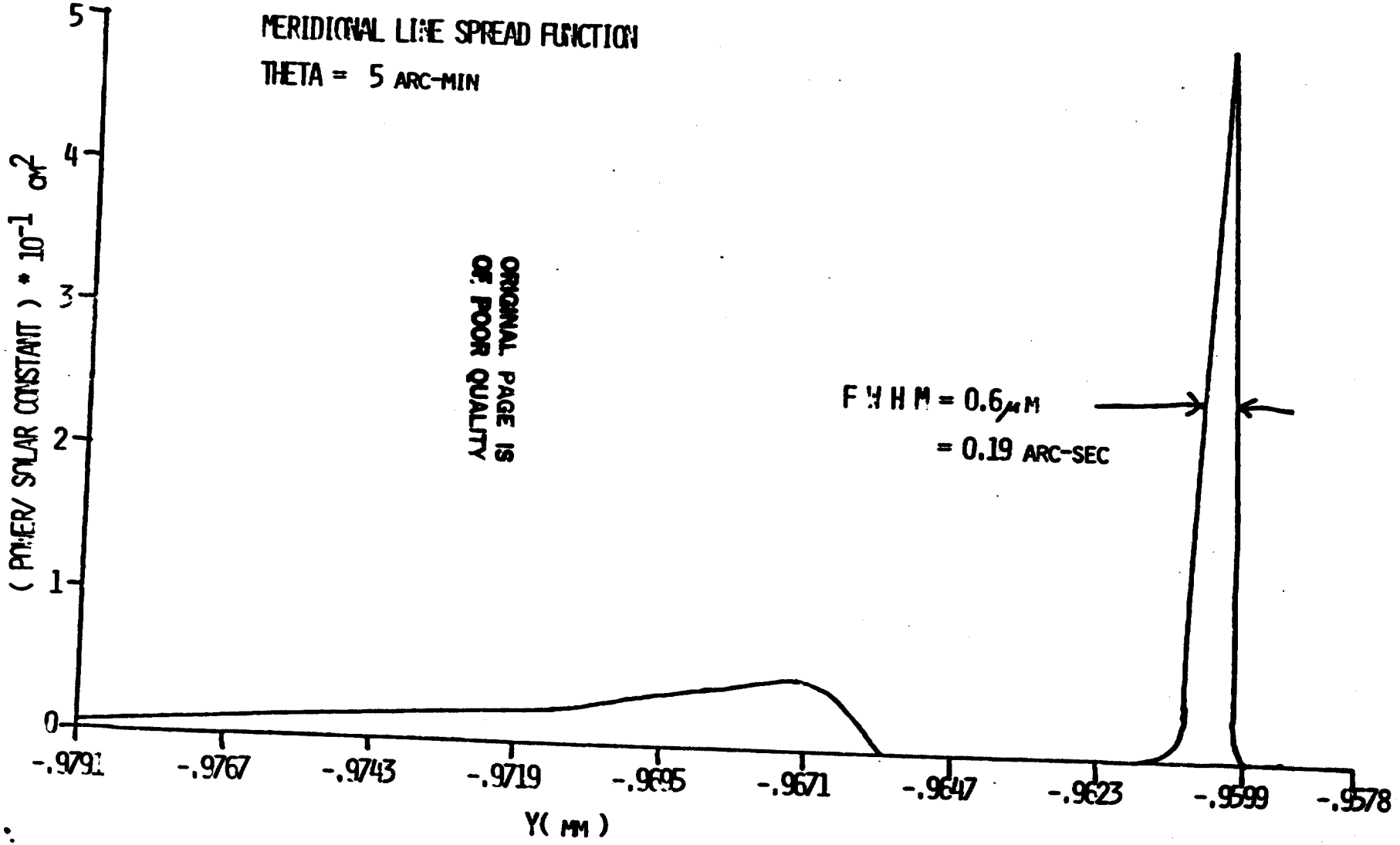






Fig. 6a

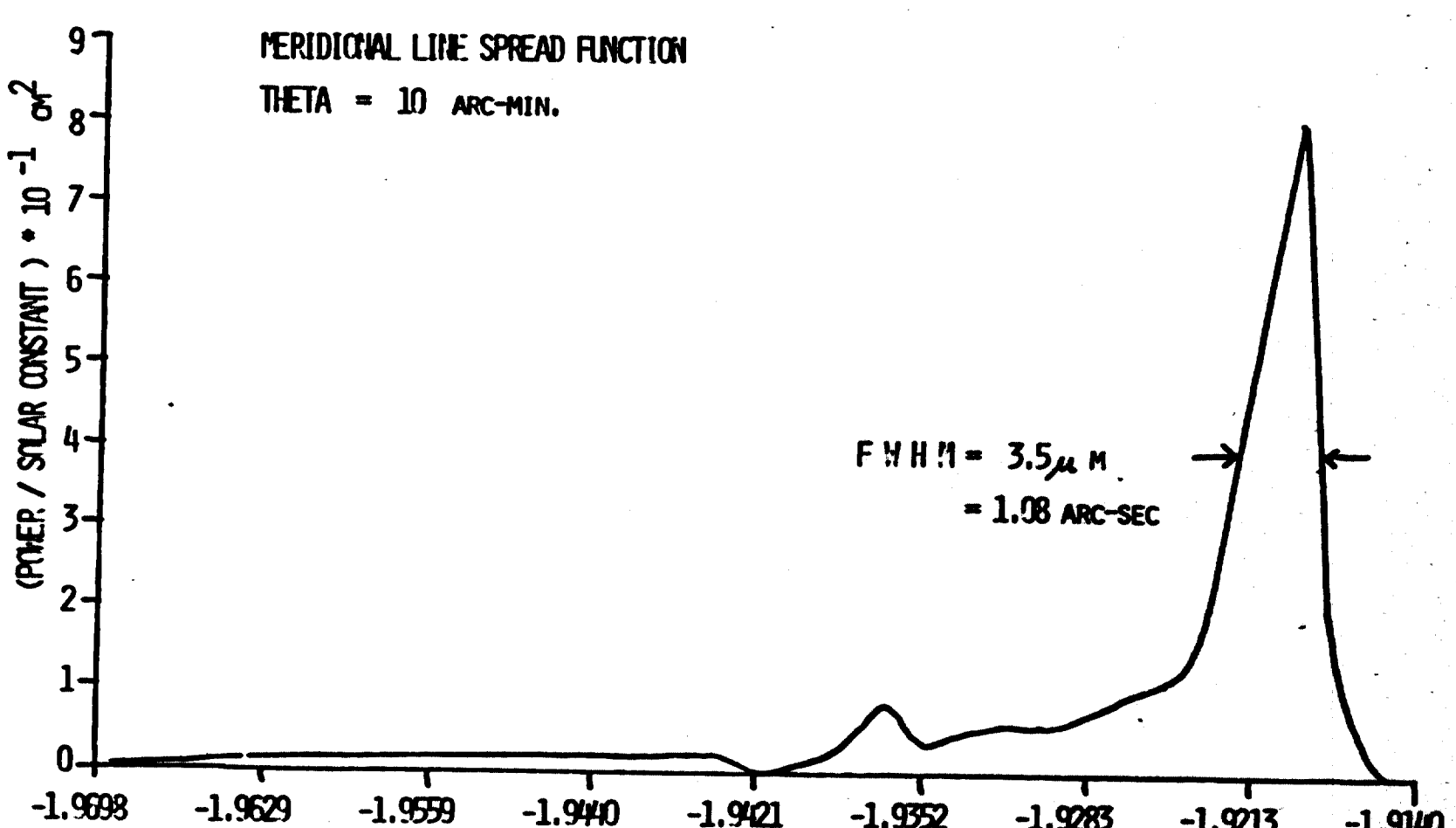
MERIDIONAL LINE SPREAD FUNCTION
THETA = 10 ARC-MIN.
(POWER / SOLAR CONSTANT) * 10^-1 cm^2
9
8
7
6
5
4
3
2
1
0
FWHM = 3.5 μM
= 1.08 ARC-SEC
-1.9698
-1.9629
-1.9559
-1.9490
-1.9421
-1.9352
-1.9283
-1.9213
-1.9140
Y ( MM )

Fig. 6b

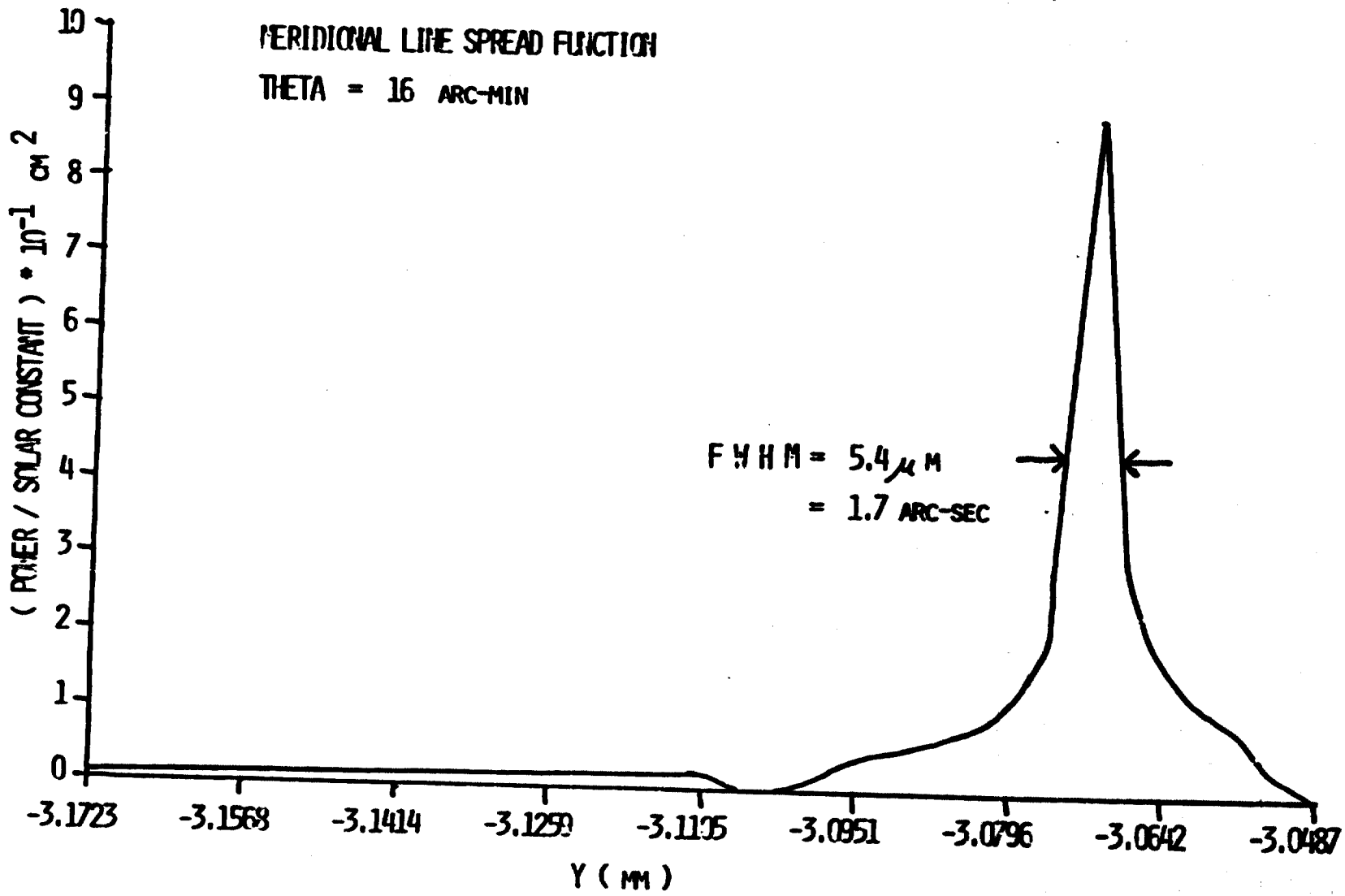
MERIDIONAL LINE SPREAD FUNCTION
THETA = 16 ARC-MIN
( POWER / SOLAR CONSTANT ) * $10^{-1}$ CM $^2$
10
9
8
7
6
5
4
3
2
1
0
FWHM = 5.4 μM
= 1.7 ARC-SEC
-3.1723
-3.1568
-3.1414
-3.1259
-3.1105
-3.0951
-3.0796
-3.0642
-3.0487
Y ( MM )

Fig. 6c

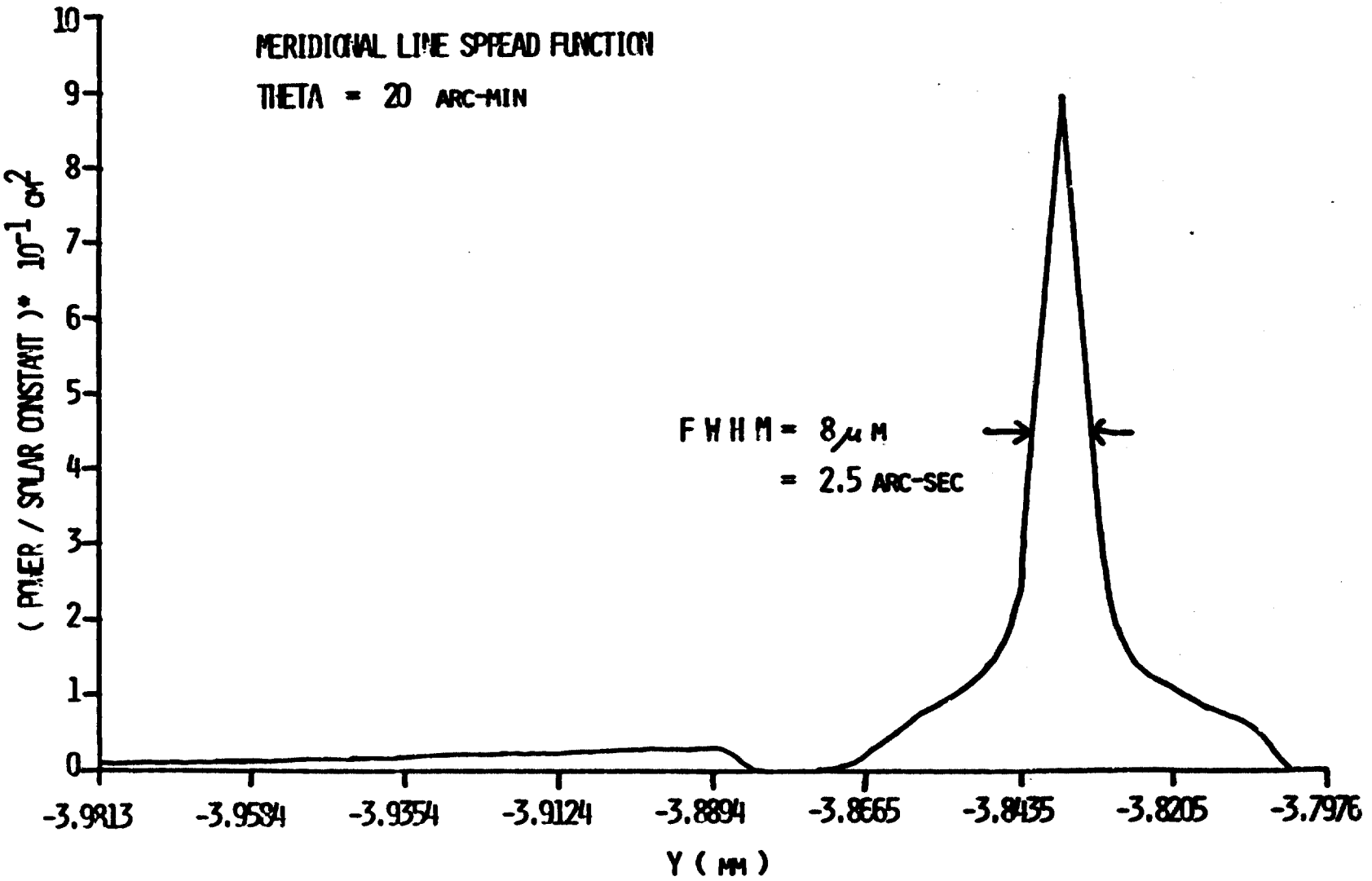
MERIDIONAL LINE SPREAD FUNCTION
THETA = 20 ARC-MIN
( PMER / SOLAR CONSTANT ) * $10^{-1}$ $cm^2$
FWHM = 8 μM
= 2.5 ARC-SEC
10
9
8
7
6
5
4
3
2
1
0
-3.9813
-3.9584
-3.9354
-3.9124
-3.8894
-3.8665
-3.8435
-3.8205
-3.7976
Y ( MM )

Fig. 6d

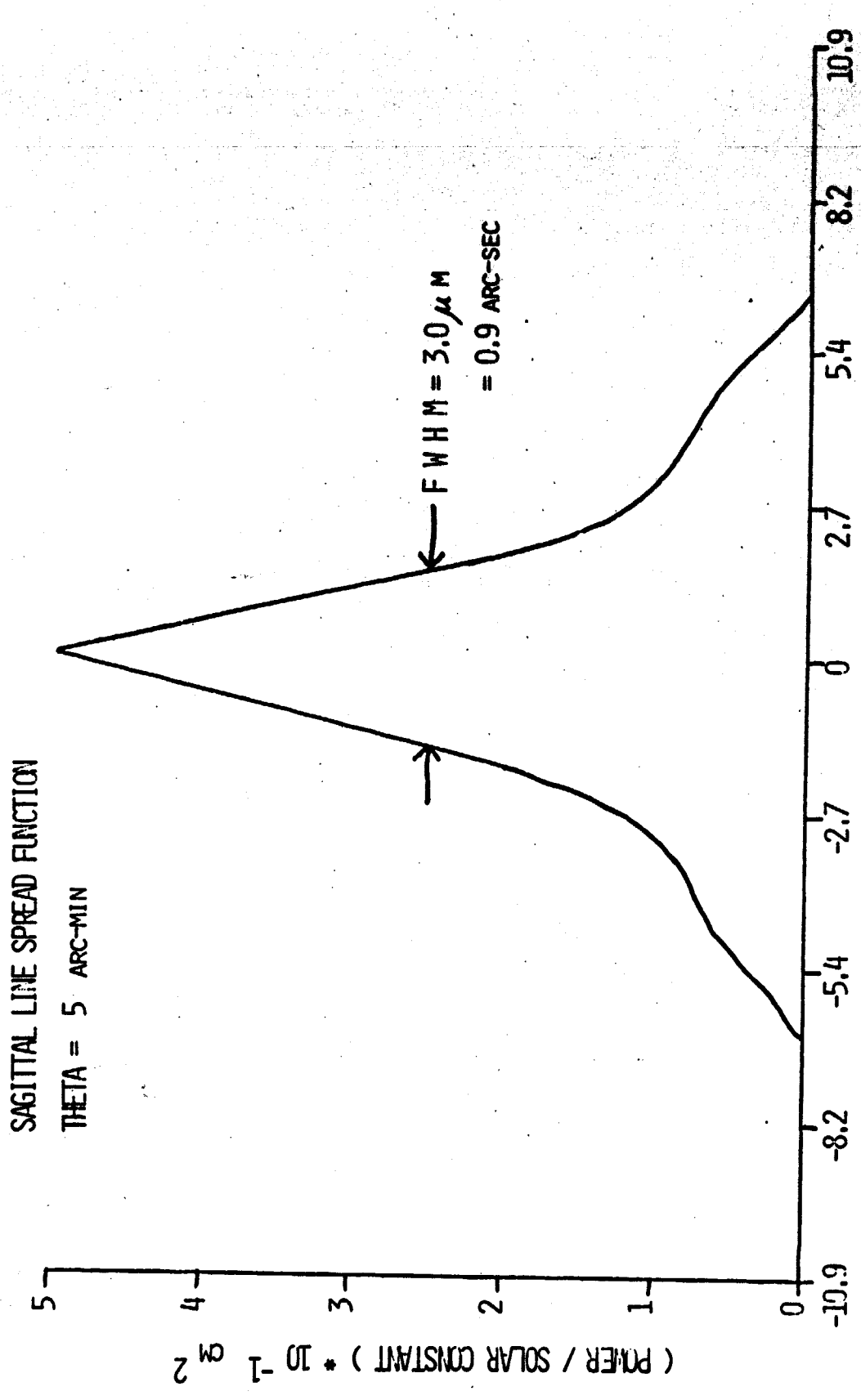
SAGITTAL LINE SPREAD FUNCTION
THETA = 5 ARC-MIN
FWHM = 3.0 μM
= 0.9 ARC-SEC
( POWER / SOLAR CONSTANT ) * 10 -1 cm 2
5
4
3
2
1
0
-10.9
-8.2
-5.4
-2.7
0
2.7
5.4
8.2
10.9
Z (μM)

Fig. 7a

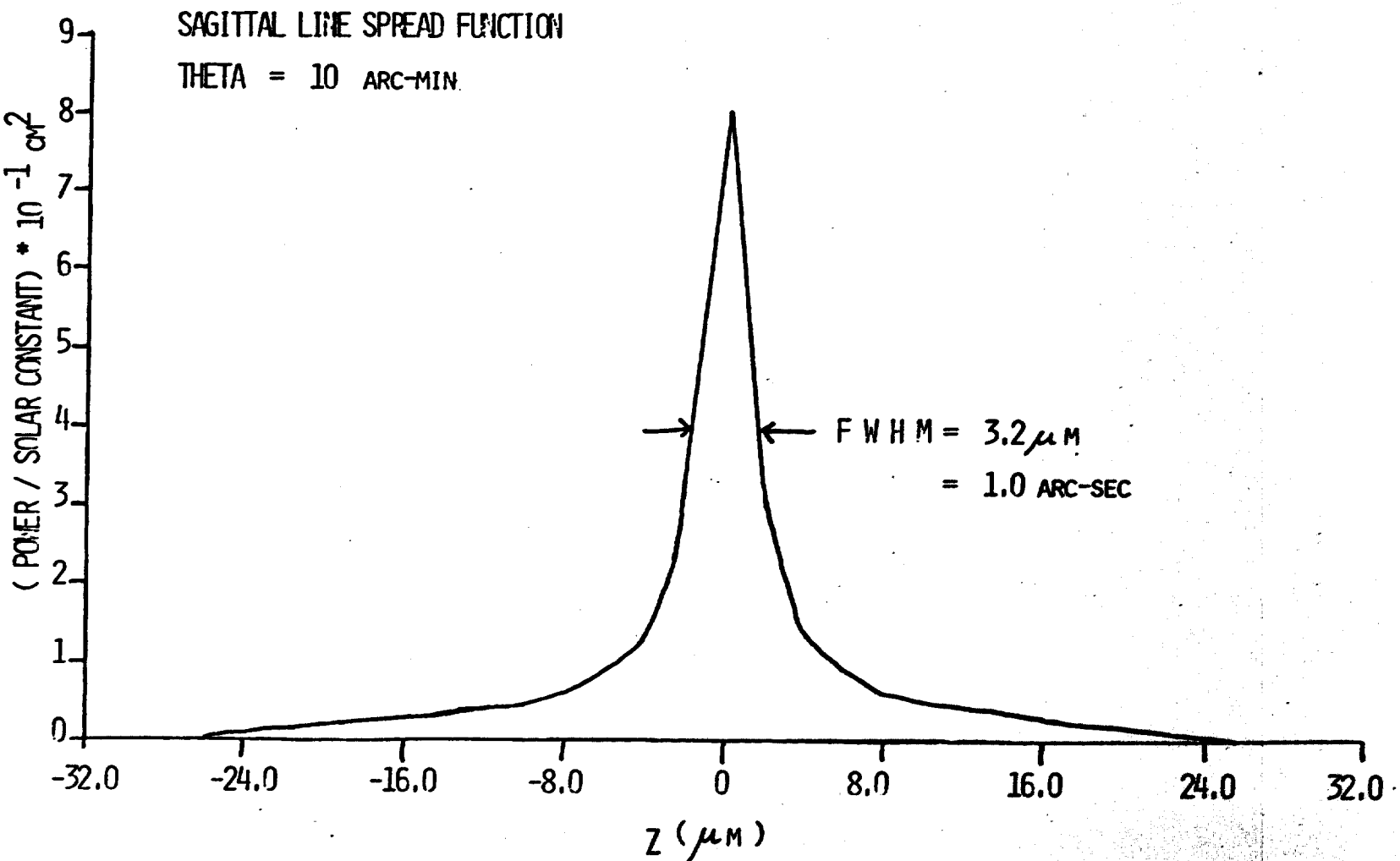
SAGITTAL LINE SPREAD FUNCTION
THETA = 10 ARC-MIN
( POWER / SOLAR CONSTANT) * 10 -1 CM2
9
8
7
6
5
4
3
2
1
0
FWHM = 3.2 μM
= 1.0 ARC-SEC
-32.0
-24.0
-16.0
-8.0
0
8.0
16.0
24.0
32.0
Z (μM)

Fig. 7b

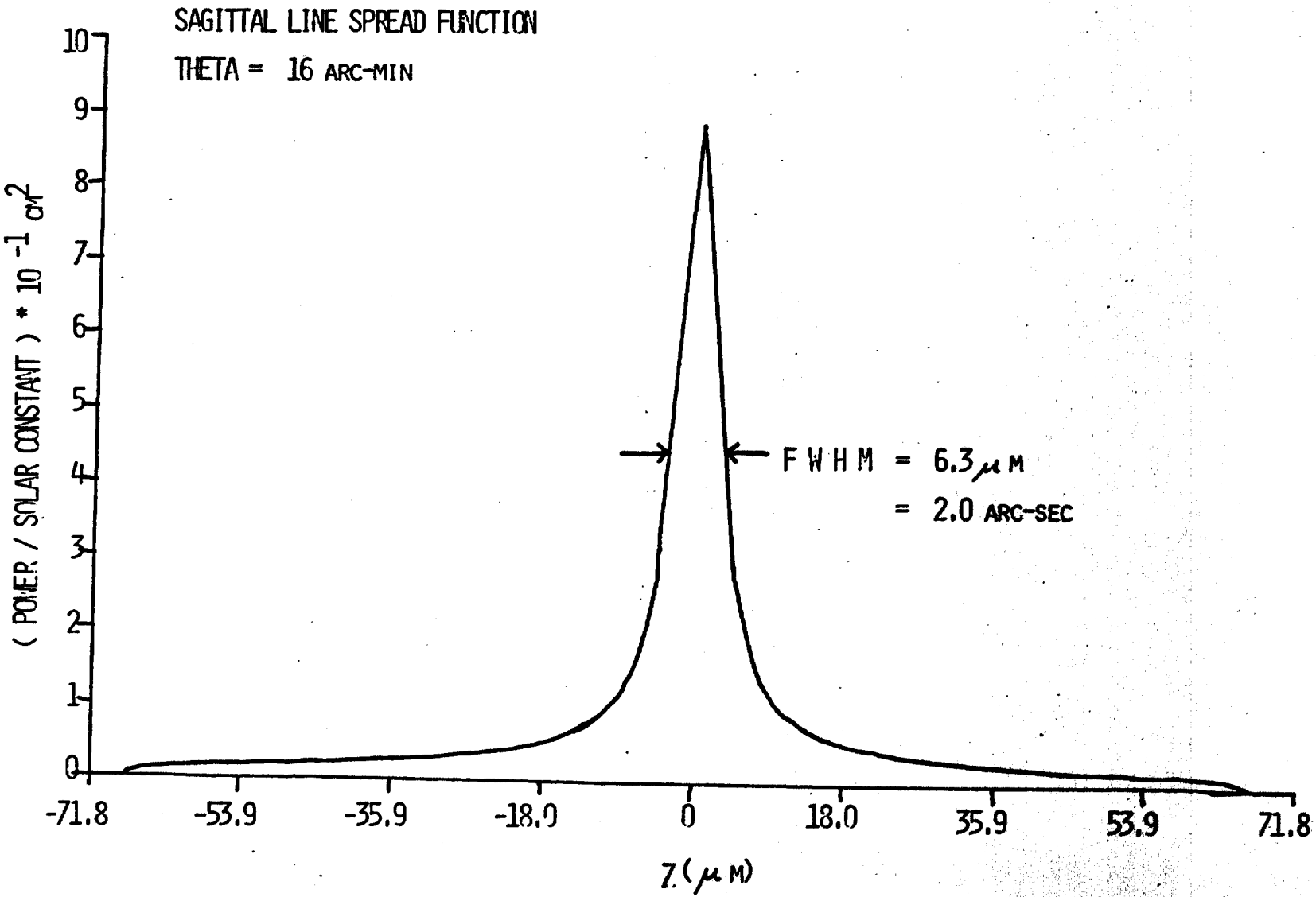
SAGITTAL LINE SPREAD FUNCTION
THETA = 16 ARC-MIN
( POWER / SOLAR CONSTANT ) * 10 -1 σx2
10
9
8
7
6
5
4
3
2
1
0
FWHM = 6.3μM
= 2.0 ARC-SEC
-71.8
-53.9
-35.9
-18.0
0
18.0
35.9
53.9
71.8
X (μM)

Fig. 7c

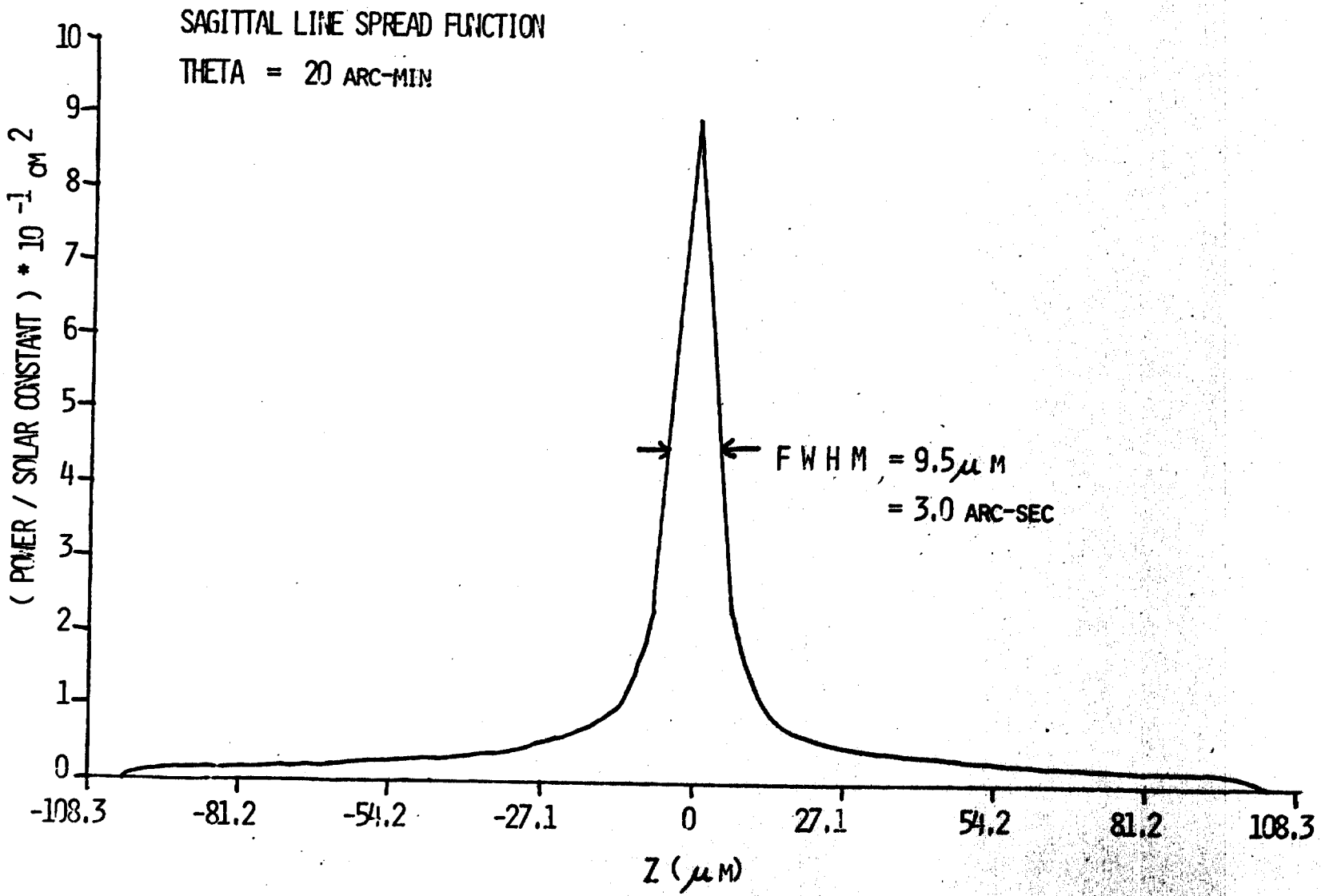
SAGITTAL LINE SPREAD FUNCTION
THETA = 20 ARC-MIN
( POWER / SOLAR CONSTANT ) * 10 -1 CM 2
10
9
8
7
6
5
4
3
2
1
0
FWHM = 9.5μM
= 3.0 ARC-SEC
-108.3
-81.2
-54.2
-27.1
0
27.1
54.2
81.2
108.3
Z (μM)

Fig. 7d

20 arc-min and less than 1 arc-sec for a field angle of 5 arc-min. It is recognized that the accuracy with which the empirical formula, Eq. 26, predicts the resolution of an x-ray telescope can be improved by correlating the observed resolution with the rms blur circle radius data for additional x-ray telescopes. This has not been done due to time constraints under the present study. However, it should be noted from Fig. 5 that the empirical formula , Eq. 26, agrees reasonably well with the FWHM results.

The discrepancy between the resolution predicted by the rms blur circle radius and the FWHM from the LSF may be understood by examining the point spread function data in more detail. It has been found that for a field angle of 16 arc-min only 30% of the incident rays intercepts the image plane within a region centered on the central peak in the point spread function of a diameter equal to the FWHM. The majority of the rays are incident upon the image plane at considerably larger distances from the central peak in LSF. Thus, the rms blur circle radius is larger than the FWHM. However, the high energy density located within the central peak of the LSF dominates the spread out backgound illumination at the detector in producing an image. Thus, the FWHM of the LSF is a more accurate measure of resolution of an x-ray telescope than the rms blur circle radius.

It has been observed by Mangus and Underwood[2] that the off axis resolution as measured by the rms blur circle radius of an x-ray telescope may be improved by shortening the length of the H mirror. Figures 8-13 present the rms blur circle radius vs. the field angle for $\ell_H$ = 9.0,8.75, 8.5, 8.25, 8.0, 7.5, respectively. By comparing Figs. 2 and 13, it is seen that the resolution may be improved by approximately 10% by shortening the length of the H mirror to 7.5 cm. and defocusing the image plane by +0.2 mm. However, the collecting area of the telescope is reduced. From Fig. 14, it is seen that when $\ell_H$ is

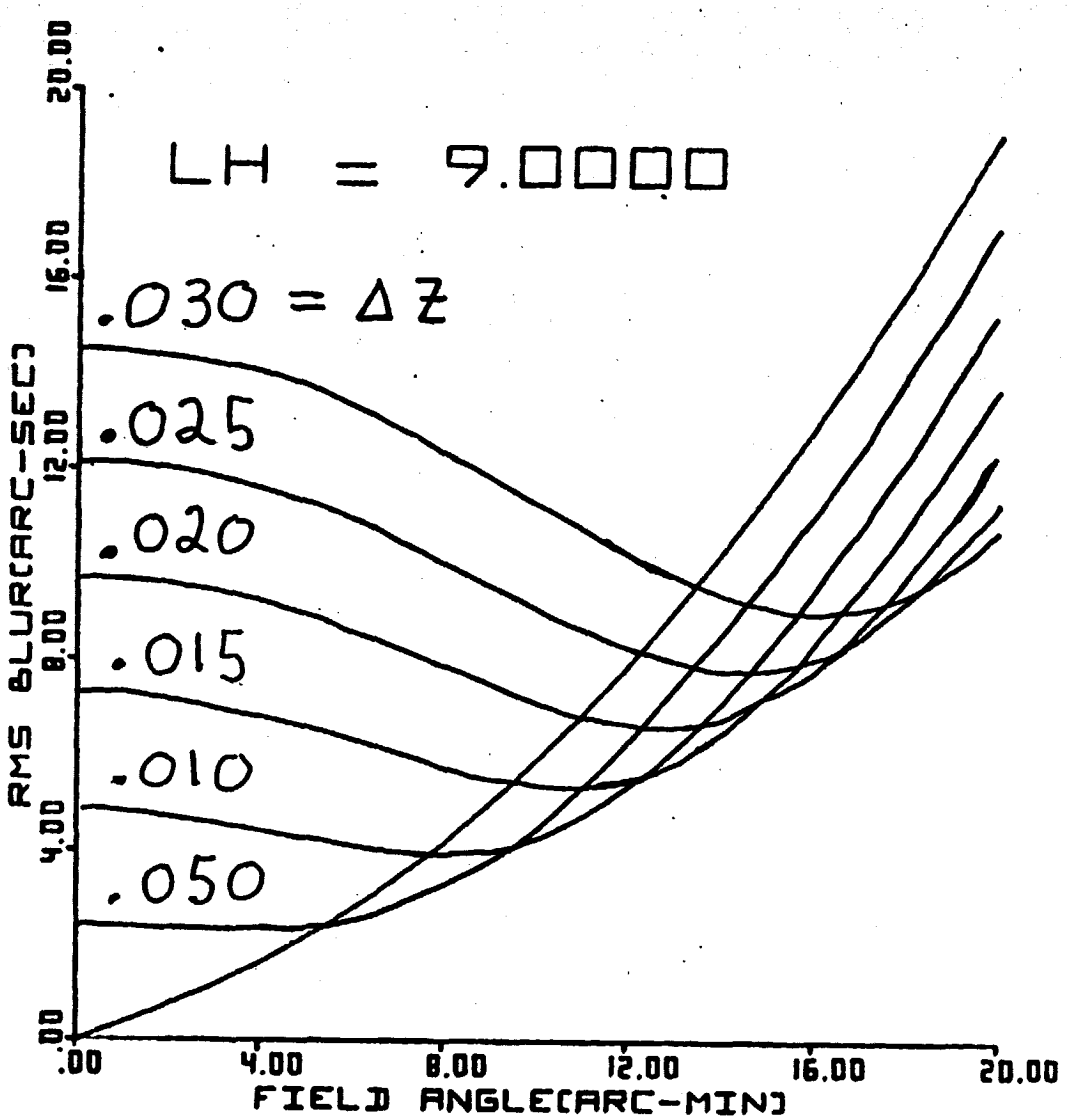
LH = 9.0000
.030 = Δ Z
.025
.020
.015
.010
.050
RMS BLUR(ARC-SEC)
20.00
16.00
12.00
8.00
4.00
.00
.00
4.00
8.00
12.00
16.00
20.00
FIELD ANGLE(ARC-MIN)

Fig. 8

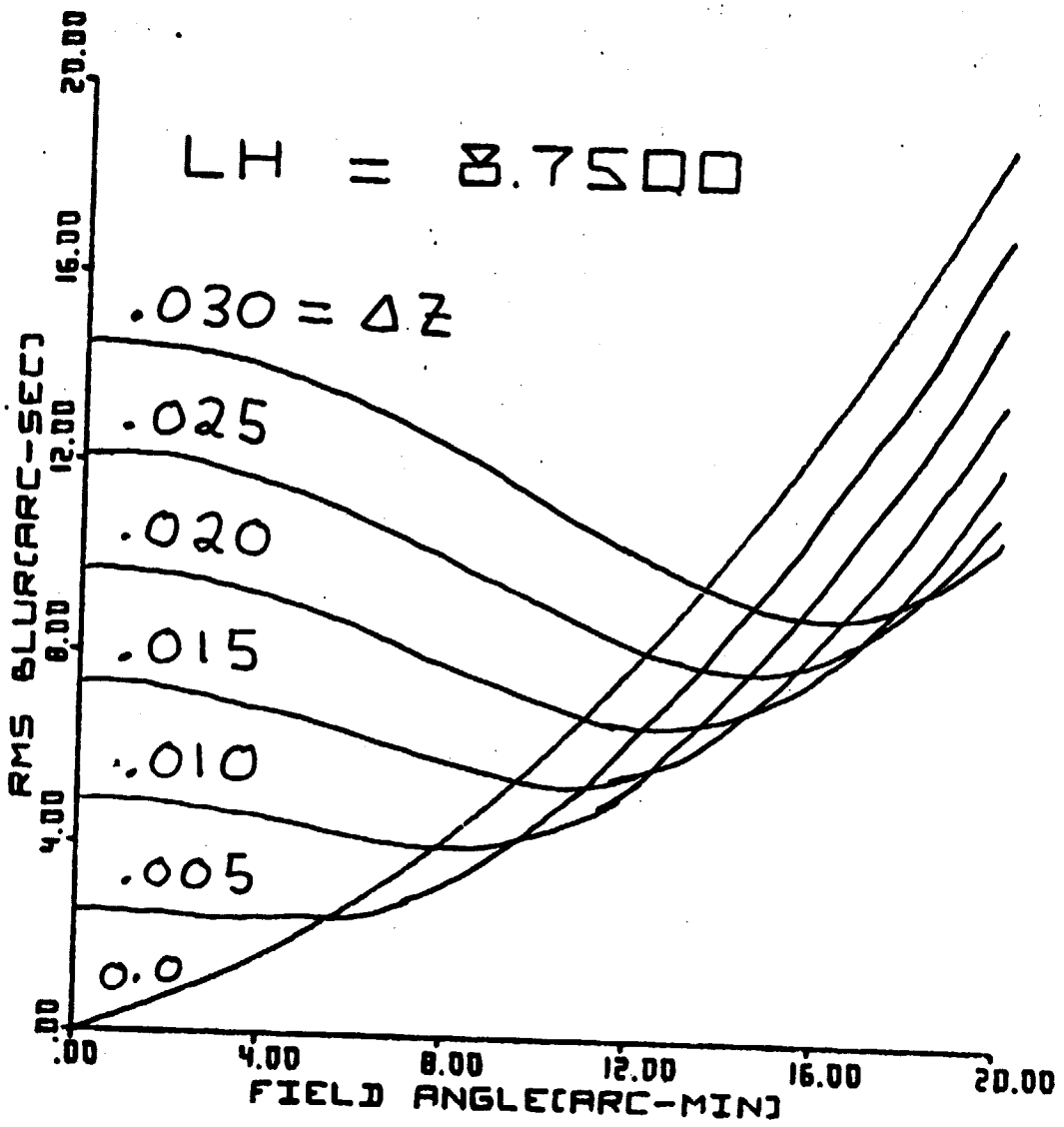
LH = 8.7500
.030 = ΔZ
.025
.020
.015
.010
.005
0.0
RMS BLUR(ARC-SEC)
20.00
16.00
12.00
8.00
4.00
.00
.00
4.00
8.00
12.00
16.00
20.00
FIELD ANGLE(ARC-MIN)

Fig. 9

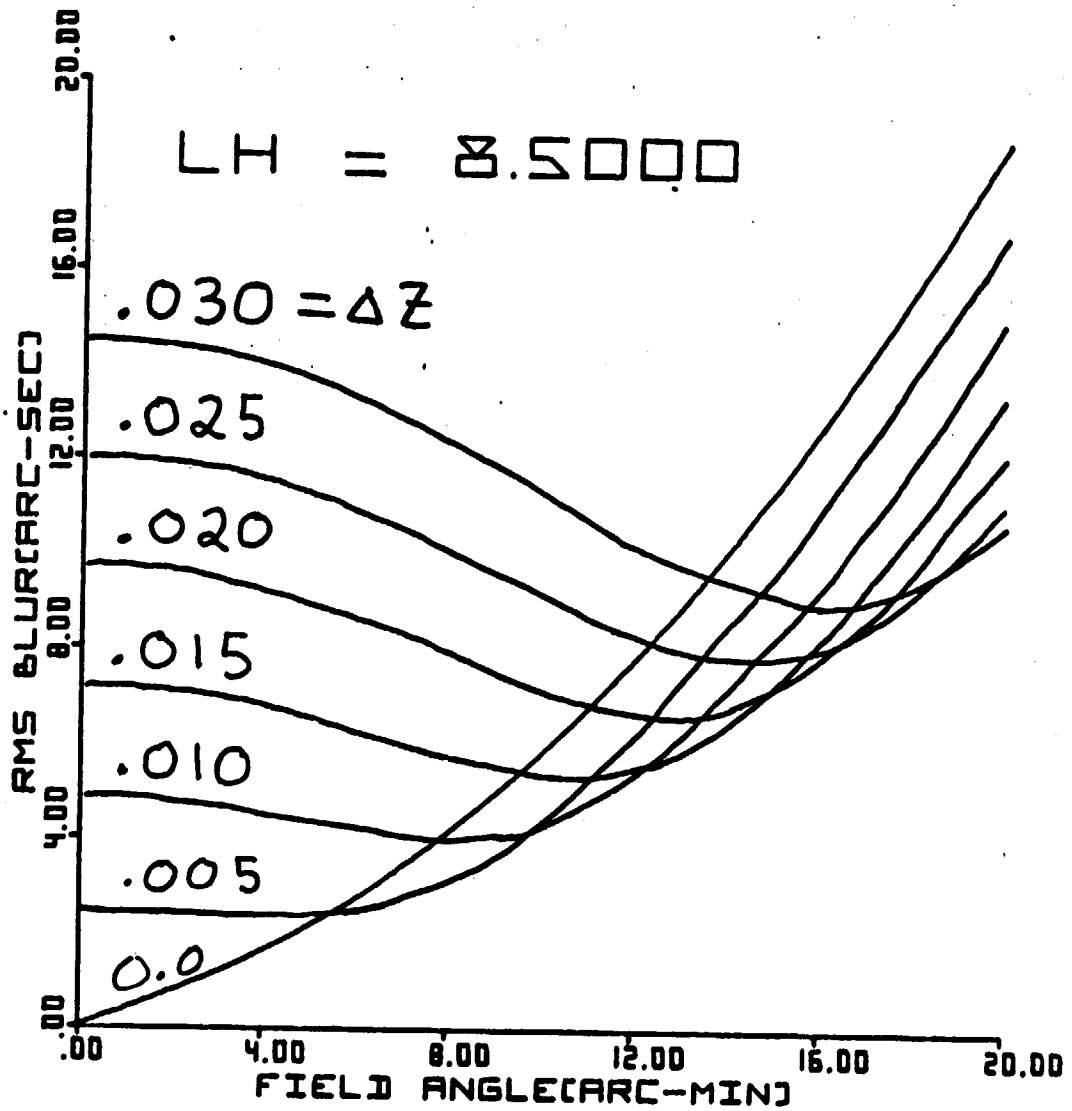
LH = 8.5000
.030 = ΔZ
.025
.020
.015
.010
.005
0.0
RMS BLUR(ARC-SEC)
20.00
16.00
12.00
8.00
4.00
.00
.00
4.00
8.00
12.00
16.00
20.00
FIELD ANGLE(ARC-MIN)

Fig. 10

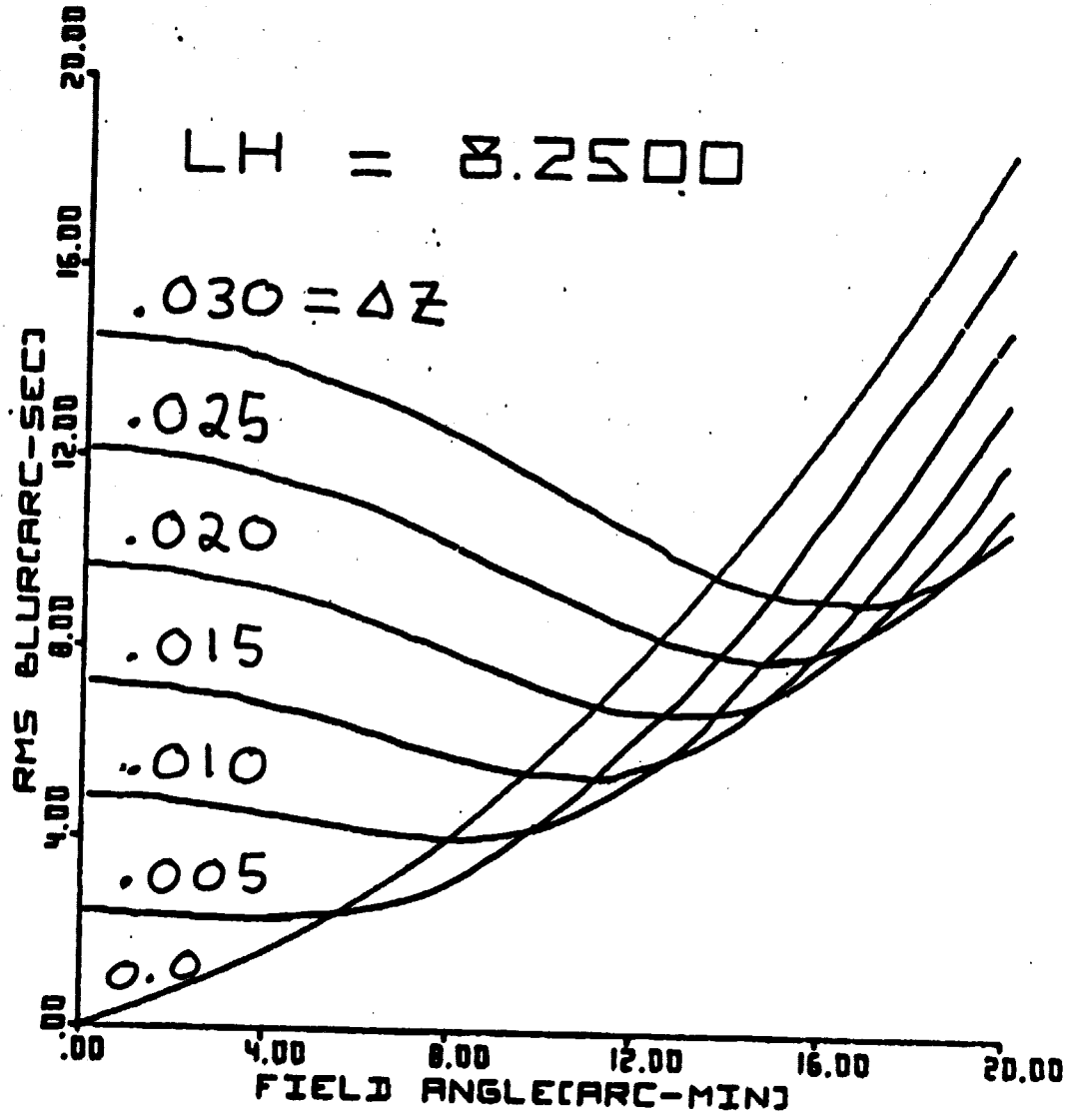
LH = 8.2500
.030 = ΔZ
.025
.020
.015
.010
.005
0.0
RMS BLUR(ARC-SEC)
FIELD ANGLE(ARC-MIN)
.00
4.00
8.00
12.00
16.00
20.00

Fig. 11

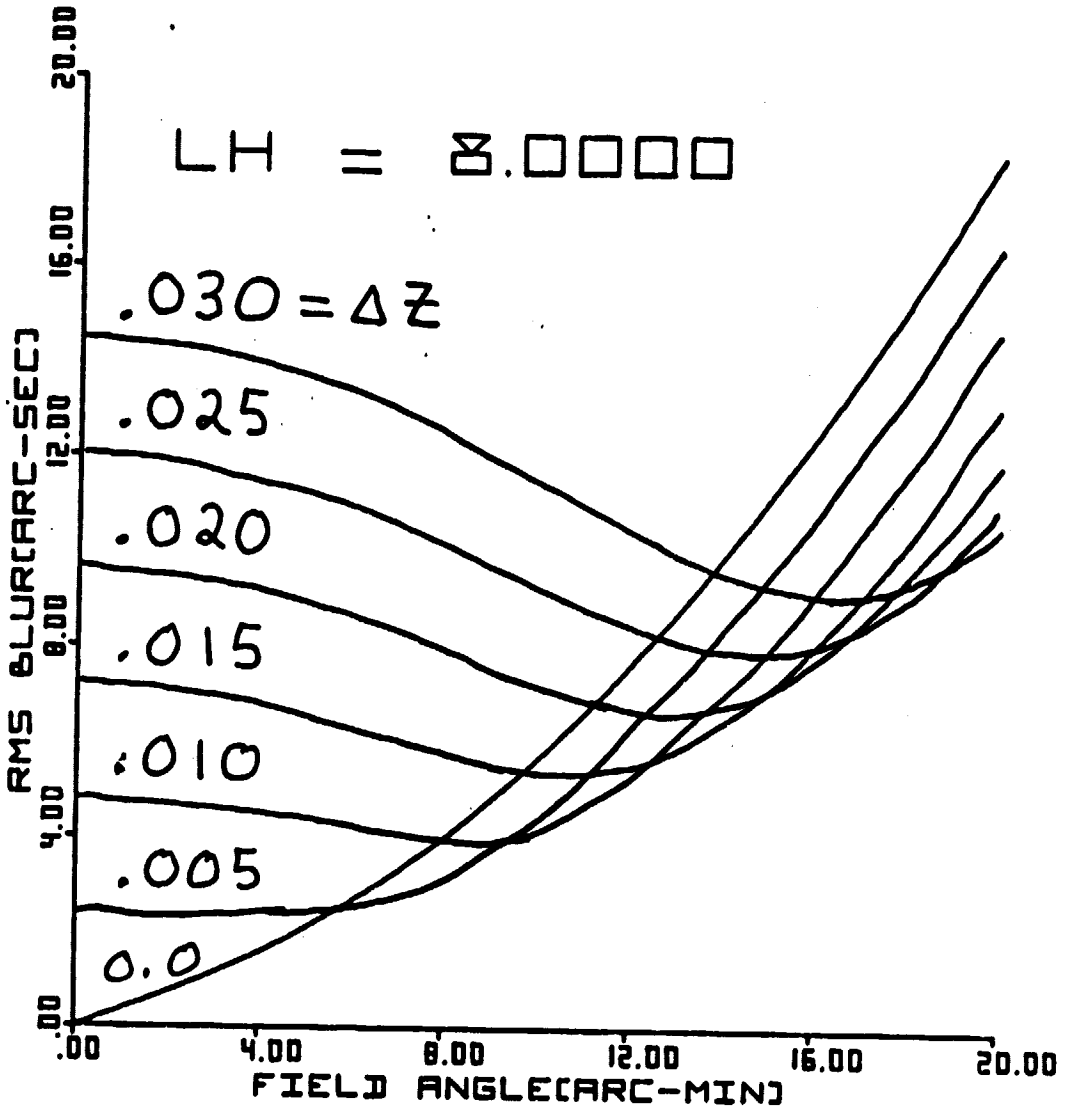
LH = 8.0000
.030 = Δz
.025
.020
.015
.010
.005
0.0
RMS BLUR(ARC-SEC)
FIELD ANGLE(ARC-MIN)
.00
4.00
8.00
12.00
16.00
20.00

Fig. 12

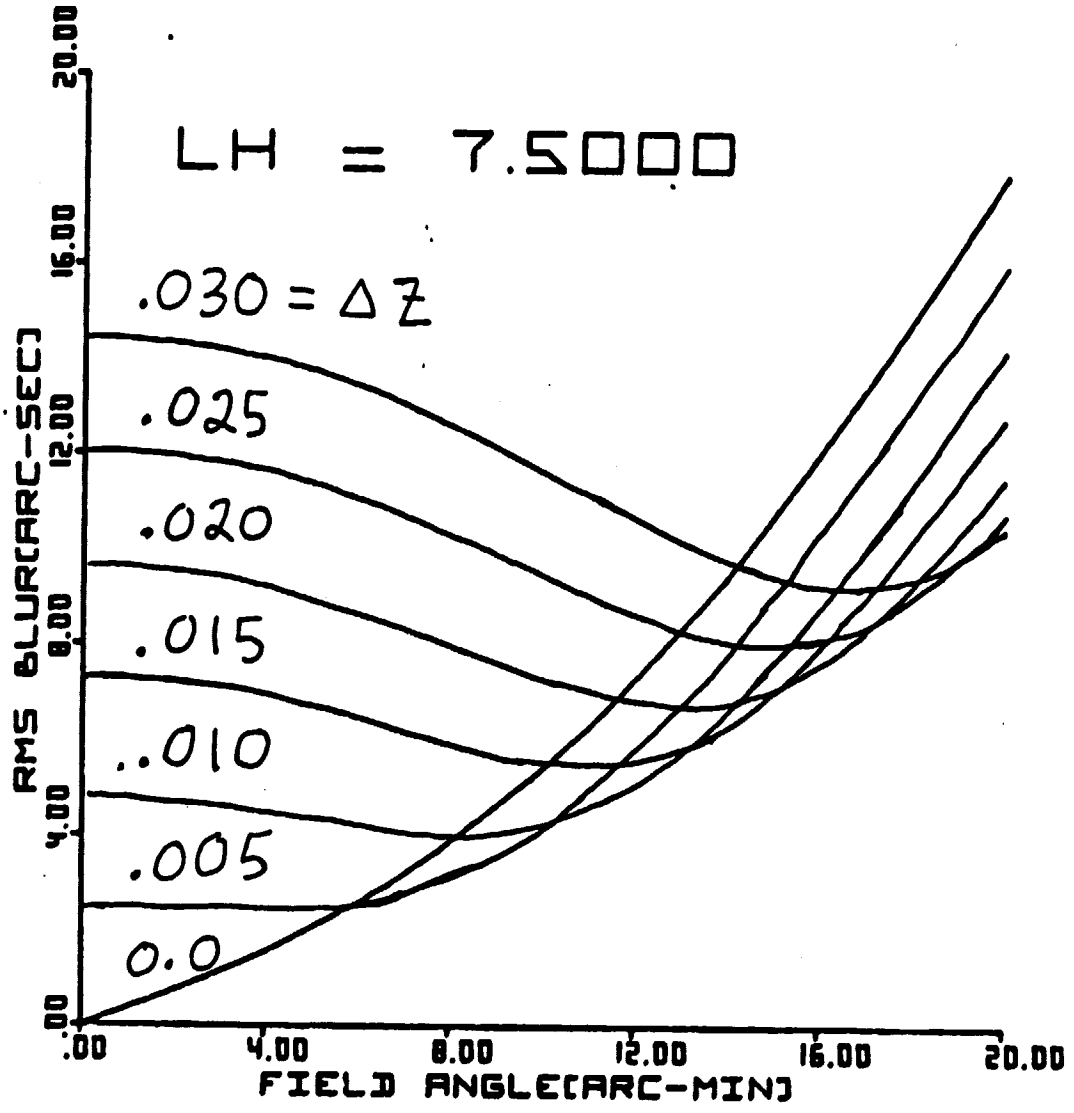
LH = 7.5000
.030 = ΔZ
.025
.020
.015
..010
.005
0.0
RMS BLUR(ARC-SEC)
FIELD ANGLE(ARC-MIN)
.00
4.00
8.00
12.00
16.00
20.00

Fig. 13

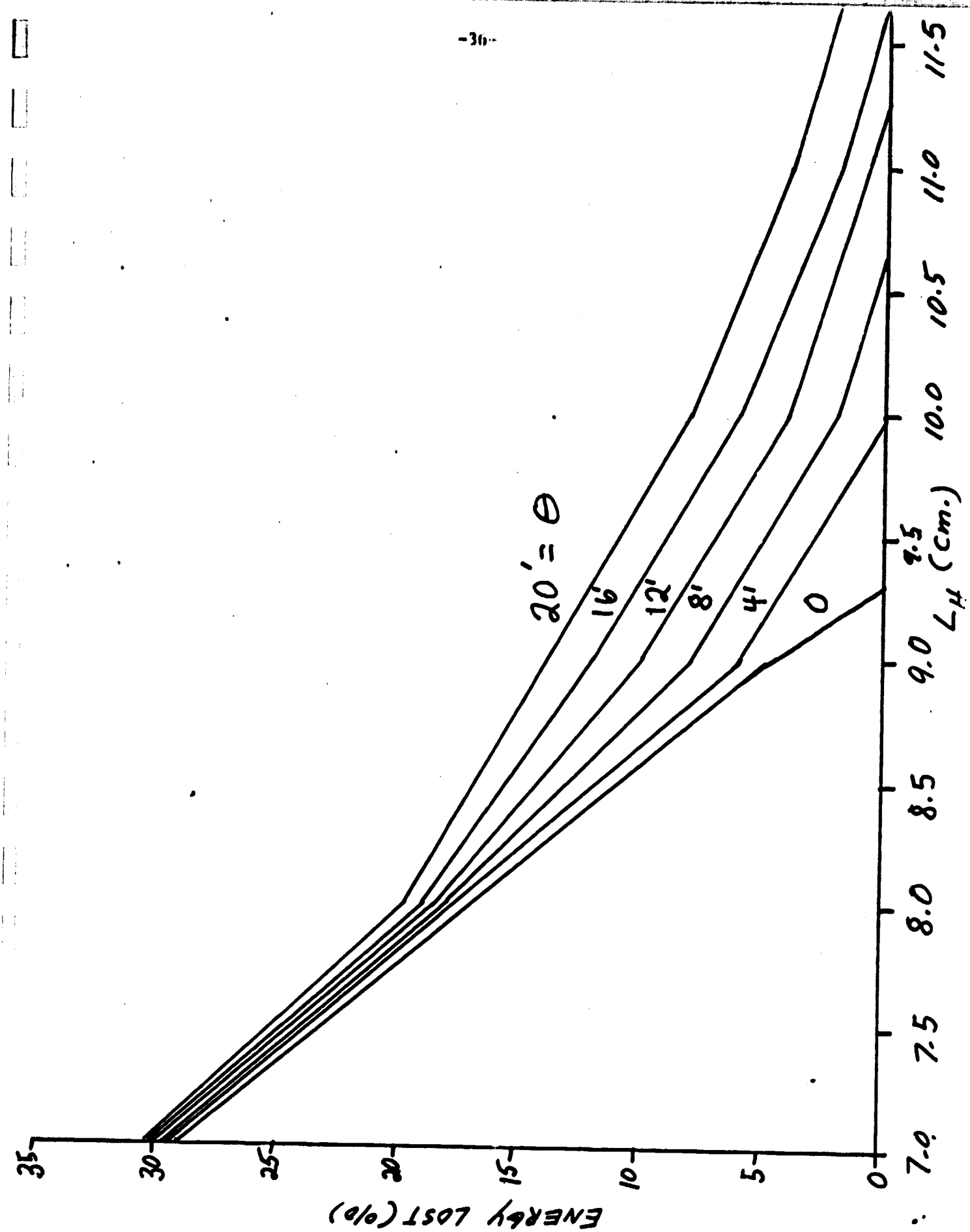
ENERGY LOST (%)
35
30
25
20
15
10
5
0
7.0
7.5
8.0
8.5
9.0
9.5
10.0
10.5
11.0
11.5
$L_\mu$ (cm.)
20° = θ
16°
12°
8°
4°
0

Fig. 14

reduced to 7.5 cm the collecting area is reduced by approximately 25% to 19 $cm^2$. Since the resolution of the proposed NOAA-MSFC GOES x-ray telescope defined by Eqs. 28 is less than 3 arc-sec at a field angle of 20 arc-min, it should not be necessary to introduce vignetting of the H mirror, to defocuse the image plane, or to use a curve image surface in order to meet the performance objectives of the GOES x-ray telescope.

In order to complete the discussion of the geometrical imaging properties of the GOES x-ray telescope with $\ell_H$ = 9.3089 cm, the rms blur circle radius as a function of the field angle on a flat and curved image surface is given in Fig. 15a. Figure 15b presents the rms blur circle radius as a function of $\Delta$ z of the optimum image surface for the field angles 4,8,12,16,20 arc-min. Figure 15c displays $\Delta$ z of the optimum image surface vs the field angle.

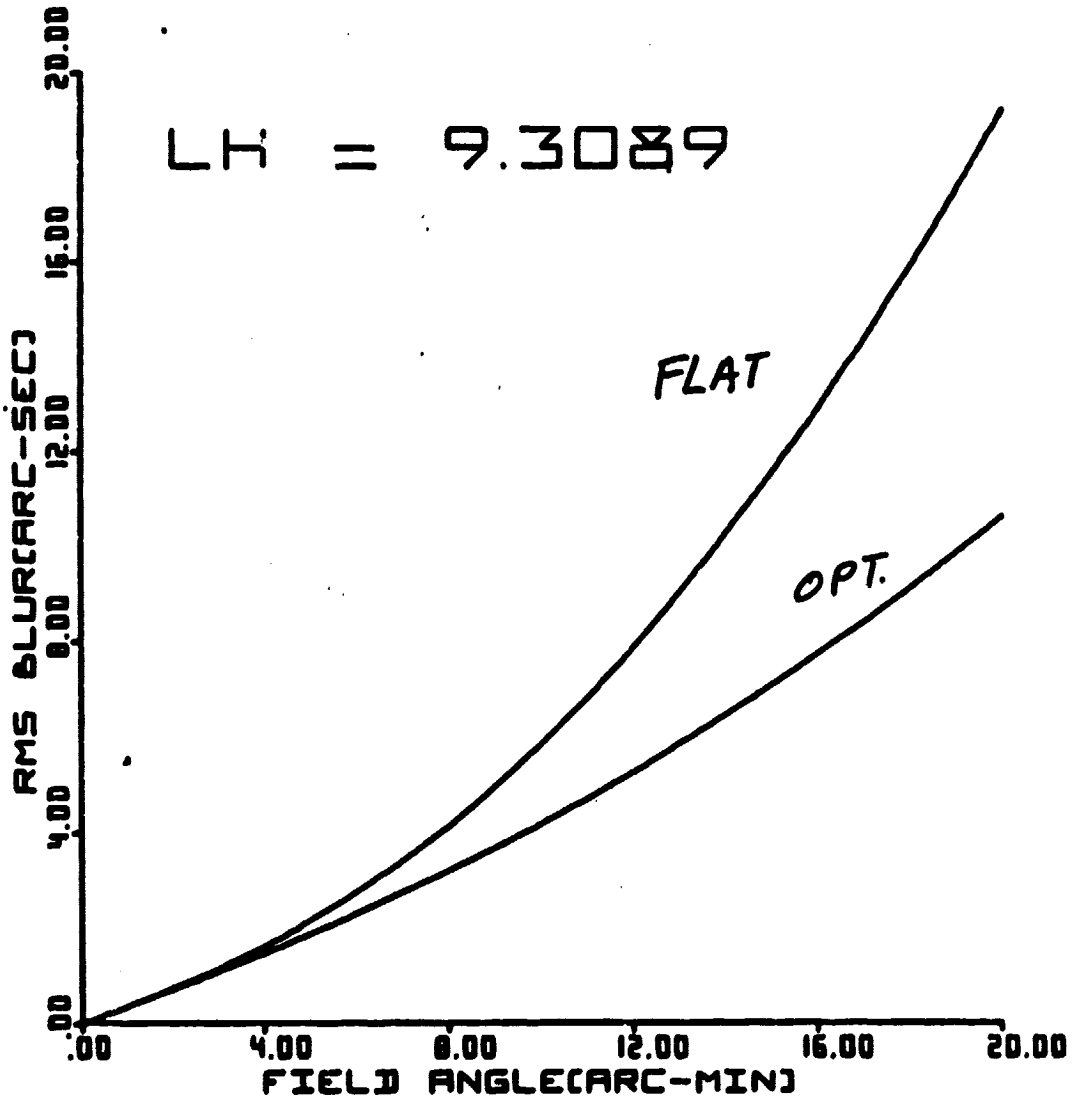
LH = 9.3089
FLAT
OPT.
RMS BLURCARC-SEC]
.00
4.00
8.00
12.00
16.00
20.00
FIELD ANGLECARC-MIN]

Fig. 15a

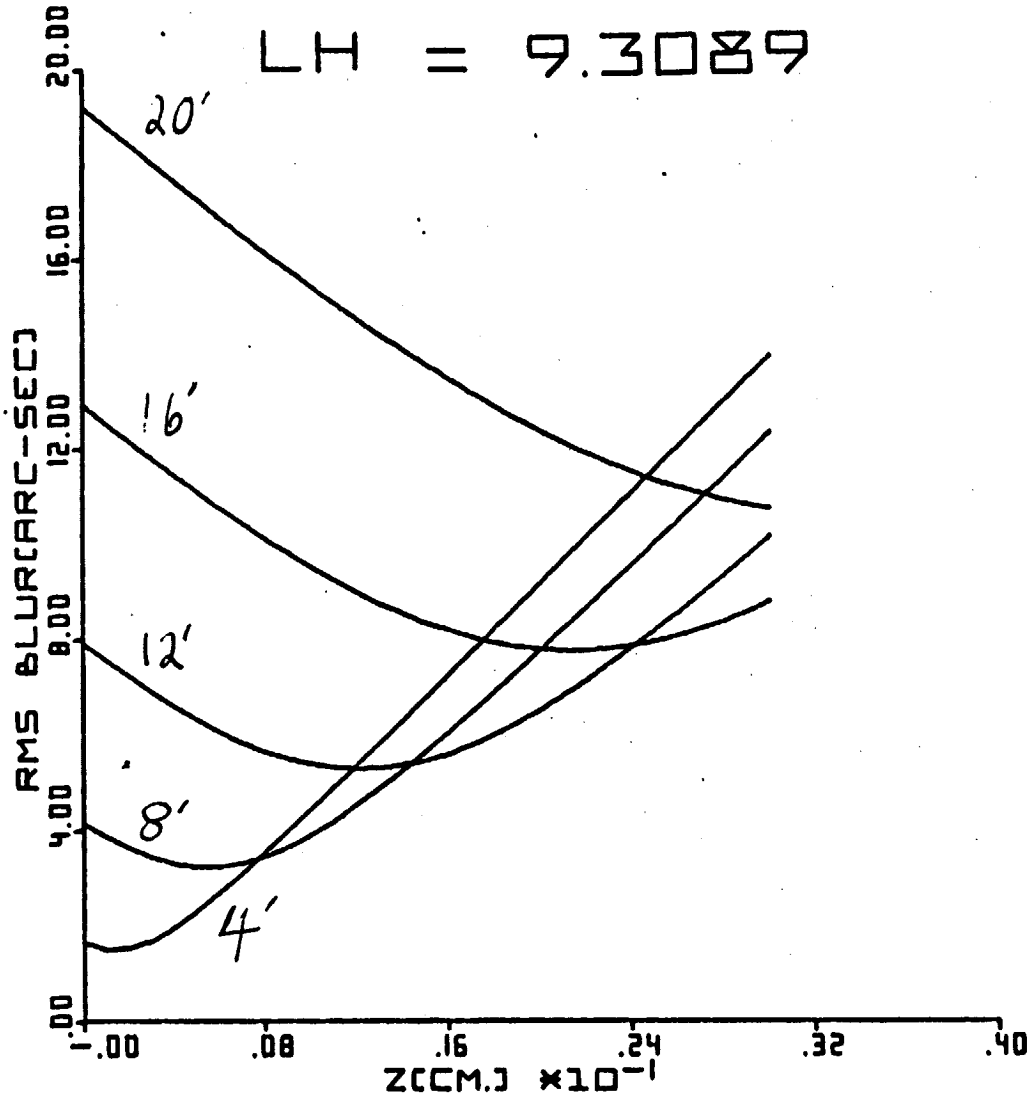
LH = 9.3089
20'
16'
12'
8'
4'
RMS BLURCARC-SEC)
20.00
16.00
12.00
8.00
4.00
.00
-.00
.08
.16
.24
.32
.40
ZCCM.) ×10⁻¹

Fig. 15b

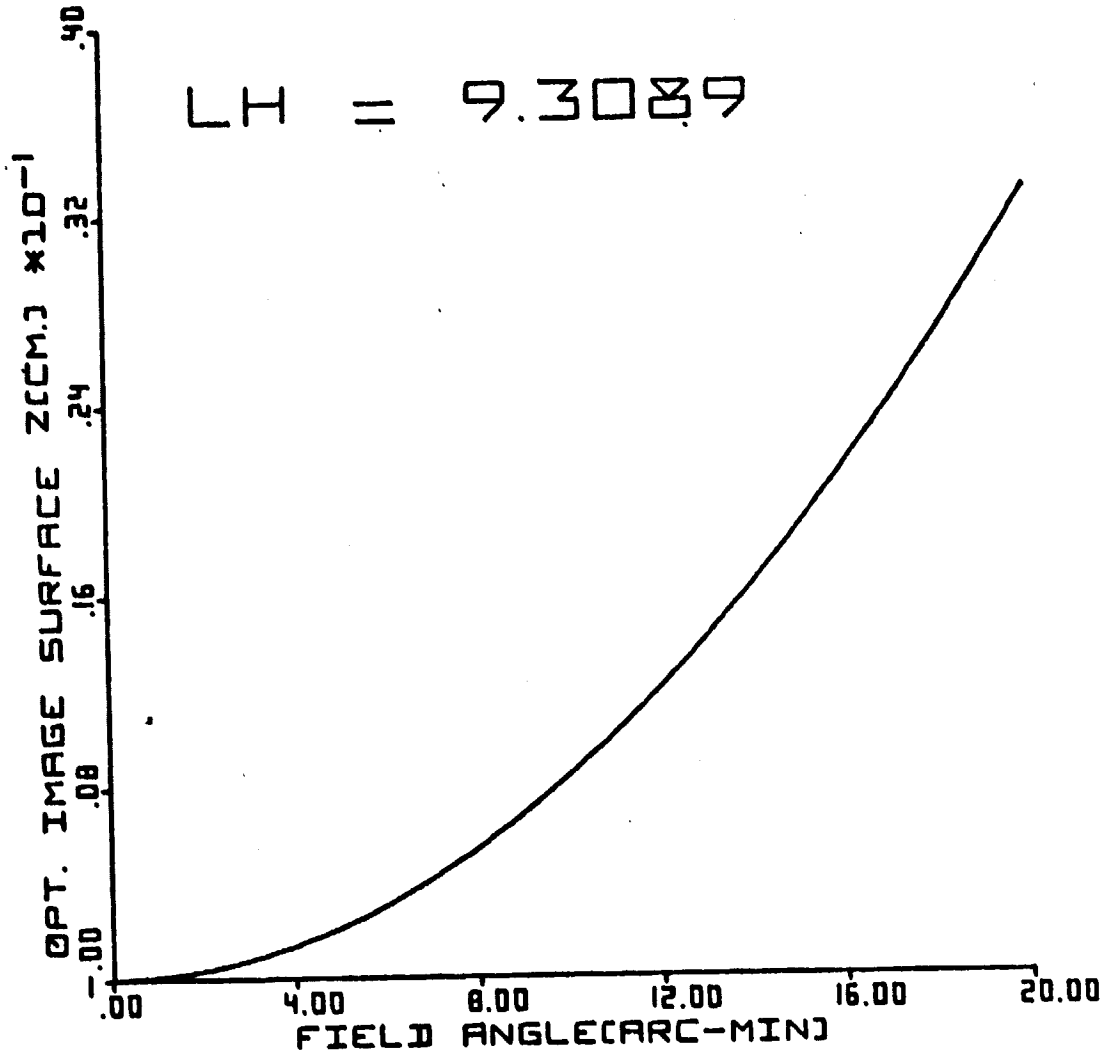
LH = 9.3089
OPT. IMAGE SURFACE Z(CM.) *10⁻¹
-.00
.08
.16
.24
.32
.40
.00
4.00
8.00
12.00
16.00
20.00
FIELD ANGLE(ARC-MIN)

Fig. 15c

## VI. Conclusion

It has been shown (Fig. 5) that a resolution better than 3 arc-sec over a $\pm$ 20 arc-min field of view should be obtained for the NOAA-MSFC GOES x-ray telescope defined by Eqs. 27-28. It has also been shown (Fig. 13) that a 10% improvement in the rms blur circle radius results when $\ell_H$ is shorten to 7.5 cm and when the image plane is defocused by 0.2mm towards the telescope. However, the collecting area of the telescope is reduced by 25% when $\ell_H$ is shorten to 7.5 cm (Fig. 14). The effect of the intentional vignetting of the H mirror on the FWHM of the LSF has not been explored. The shape of the optimum curved image surface based on the rms blur circle analysis has been evaluated (Fig. 15c).

TASK A-C have been fully addressed and the results are presented in sections II-V of this report. It is the conclusion of this study that the proposed NOAA-MSFC GOES x-ray telescope defined by Eqs. 27-28 should meet the performance objectives for the resolution and collecting area which have been setforth by MSFC technical personnel for this project. In order to complete TASK D, it is necessary for MSFC technical personnel to provide the format information required to generate the computer magnetic tape of the mirror radii as a function of the position along the optical axis for use in the diamond turning activity. Since the format information for diamond turning activities is not currently available from MSFC, the principal investigator proposes to complete TASK D after the submission of the final report,as soon as the format information is delivered to the principal investigator.

## REFERENCE


1. L. P. VanSpeybroech and R. C. Chase, APPLIED OPTICS, 11.2, 440 (1972)

2. J. D. Mangus and J. H. Underwood, APPLIED OPTICS, 8.1, 95 (1969)

3. J. W. Foreman, jr, G. W. Hunt, E. K. Lawson, "Analytical Study of the Imaging Characteristics of the Goddard ATM x-ray Telescope," SP-505-0279, Space Support Division, Sperry Rand Corporation, Huntsville, AL (1969).

4. R. J. Gagnon, JOSA, 58.8 (1968)

5. W. Werner, APPLIED OPTICS, 16.3, 764 (1977).

6. Experimental resolution data for S-056 x-ray telescope was provided Richard B. Hoover, Marshall Space Flight Center, AL.

## APPENDIX A: Alternate Mirror Designs for the GOES X-ray Telescope

An analysis of the empirical formulas of VanSpeybroeck and Chase[1] for the resolution of a telescope on a flat image plane as a function of the collecting area is given in this section. Specifically, the rms blur circle radius, $\sigma_D$, (Eq. 16 where Eq. 22 is used for $\ell_F$) has been plotted as a function of the collecting area for maximum glancing angles, $\theta_m$ = 110,120,130,140,150 arc-min. Figures A-1a,b,c,d are plots of $\sigma_D$ vs the collecting area for field angles 5,10,16,20 arc-min. In Fig. A-1c for $\theta$ = 16 arc-min, it is seen that a rms blur circle radius of 20 arc-sec may be achieved at $\theta_m$ = 130 arc-min and a collecting area of 19 $cm^2$, which is consistant with the results of the extensive ray trace described in section V. Minor improvements may be expected over those contained in Figs. A-1 when defocusing and vignetting of the H mirror are performed. For convenience, the focal length f from Eq. 21 as a function of A, $\theta_m$, and $\ell_T$ is presented in Fig. A-2. In order to translate specific values of A and $\theta_m$ from Figs. A-1a-d into corresponding focal length, one uses Fig. A-2.

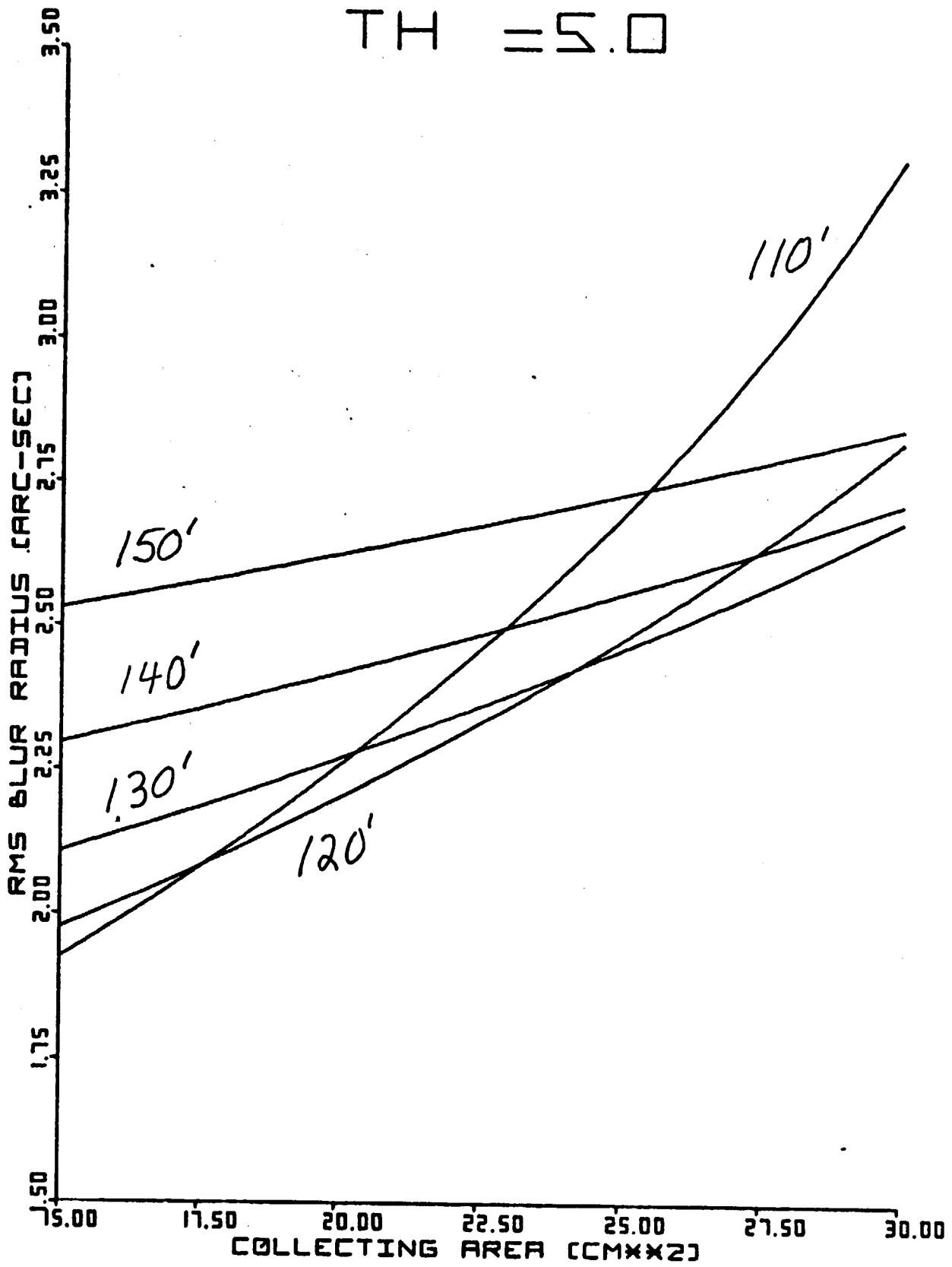
TH =5.0
RMS BLUR RADIUS (ARC-SEC)
3.50
3.25
3.00
2.75
2.50
2.25
2.00
1.75
1.50
110'
150'
140'
130'
120'
15.00
17.50
20.00
22.50
25.00
27.50
30.00
COLLECTING AREA (CM**2)

Fig. A-1a

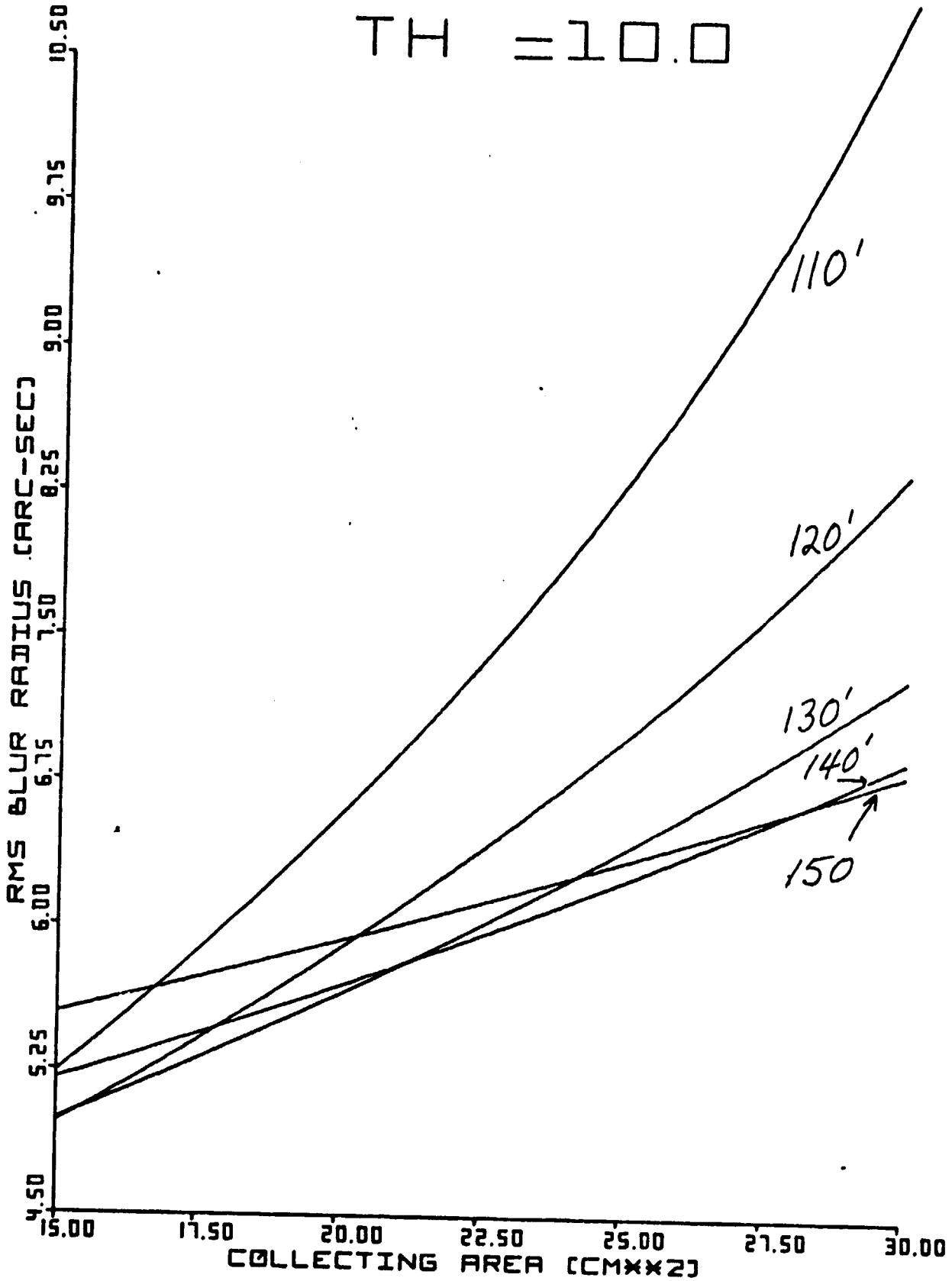
TH =10.0
RMS BLUR RADIUS (ARC-SEC)
10.50
9.75
9.00
8.25
7.50
6.75
6.00
5.25
4.50
15.00
17.50
20.00
22.50
25.00
27.50
30.00
COLLECTING AREA (CM**2)
110'
120'
130'
140'
150

Fig. A-1b

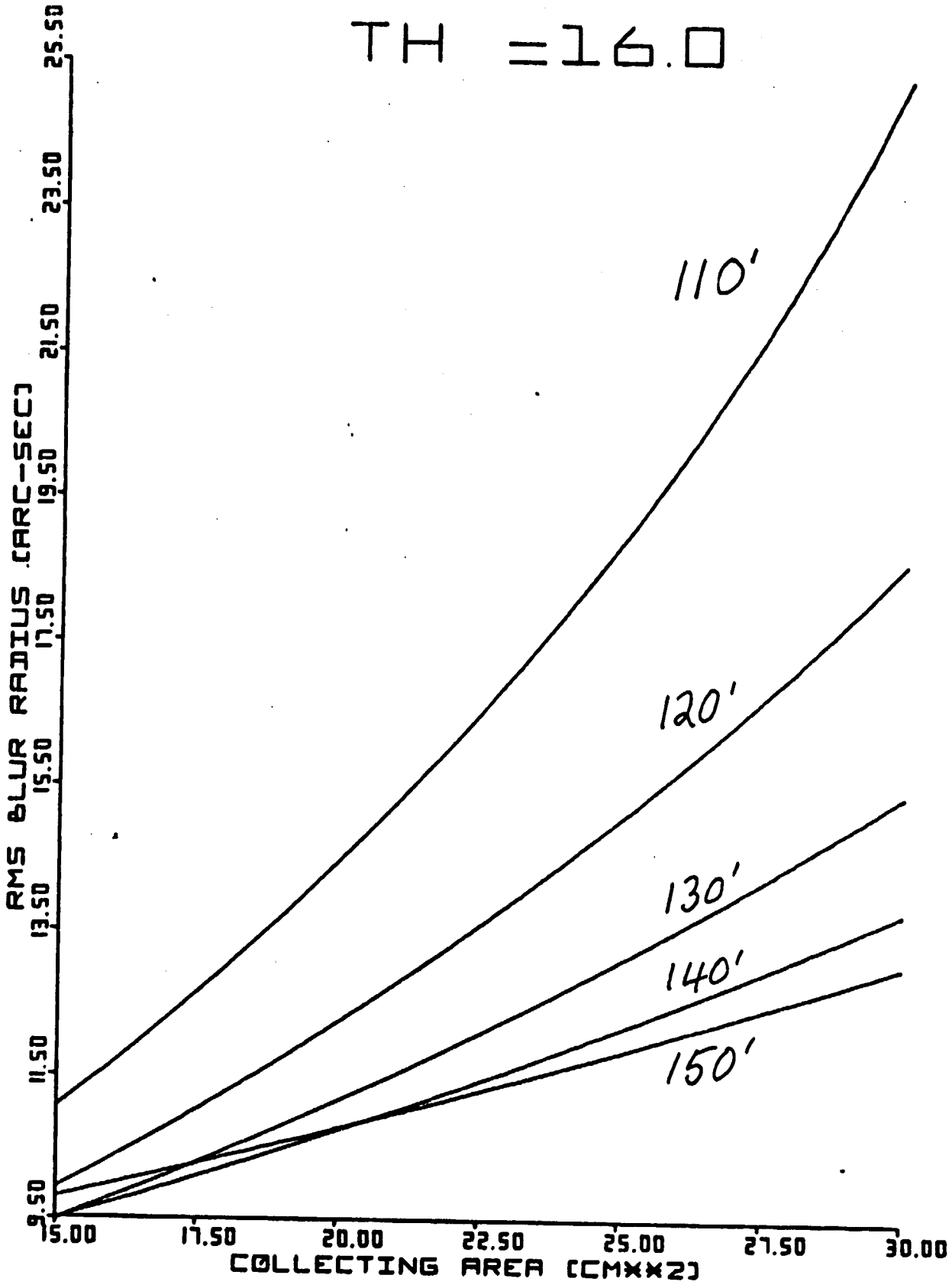
TH =16.0
RMS BLUR RADIUS (ARC-SEC)
25.50
23.50
21.50
19.50
17.50
15.50
13.50
11.50
9.50
15.00
17.50
20.00
22.50
25.00
27.50
30.00
COLLECTING AREA (CM**2)
110'
120'
130'
140'
150'

Fig. A-1c

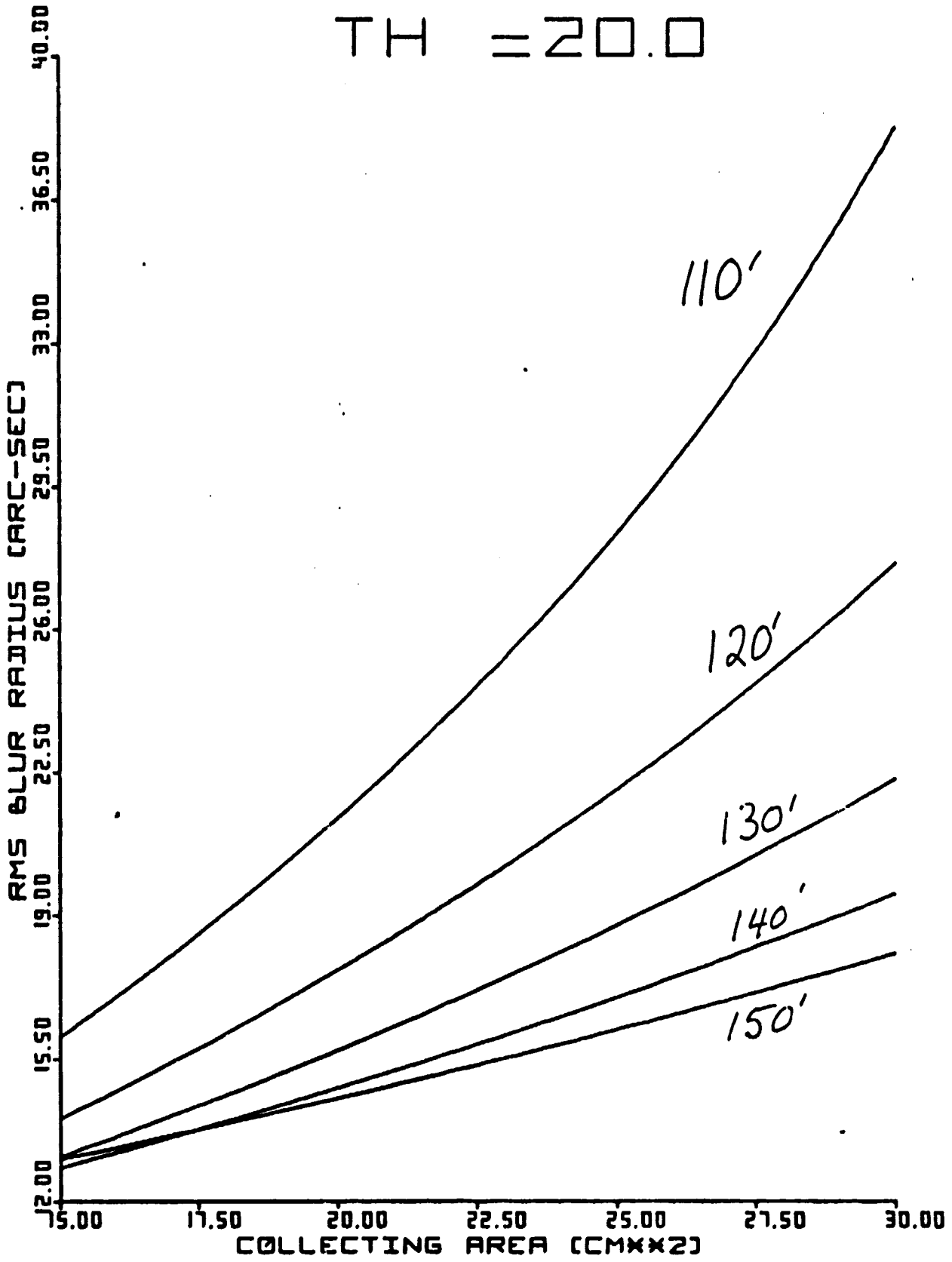
TH =20.0
RMS BLUR RADIUS (ARC-SEC)
40.00
36.50
33.00
29.50
26.00
22.50
19.00
15.50
12.00
110'
120'
130'
140'
150'
15.00
17.50
20.00
22.50
25.00
27.50
30.00
COLLECTING AREA (CM**2)

Fig. A-1d

$\ell_T = 76.2$ cm.

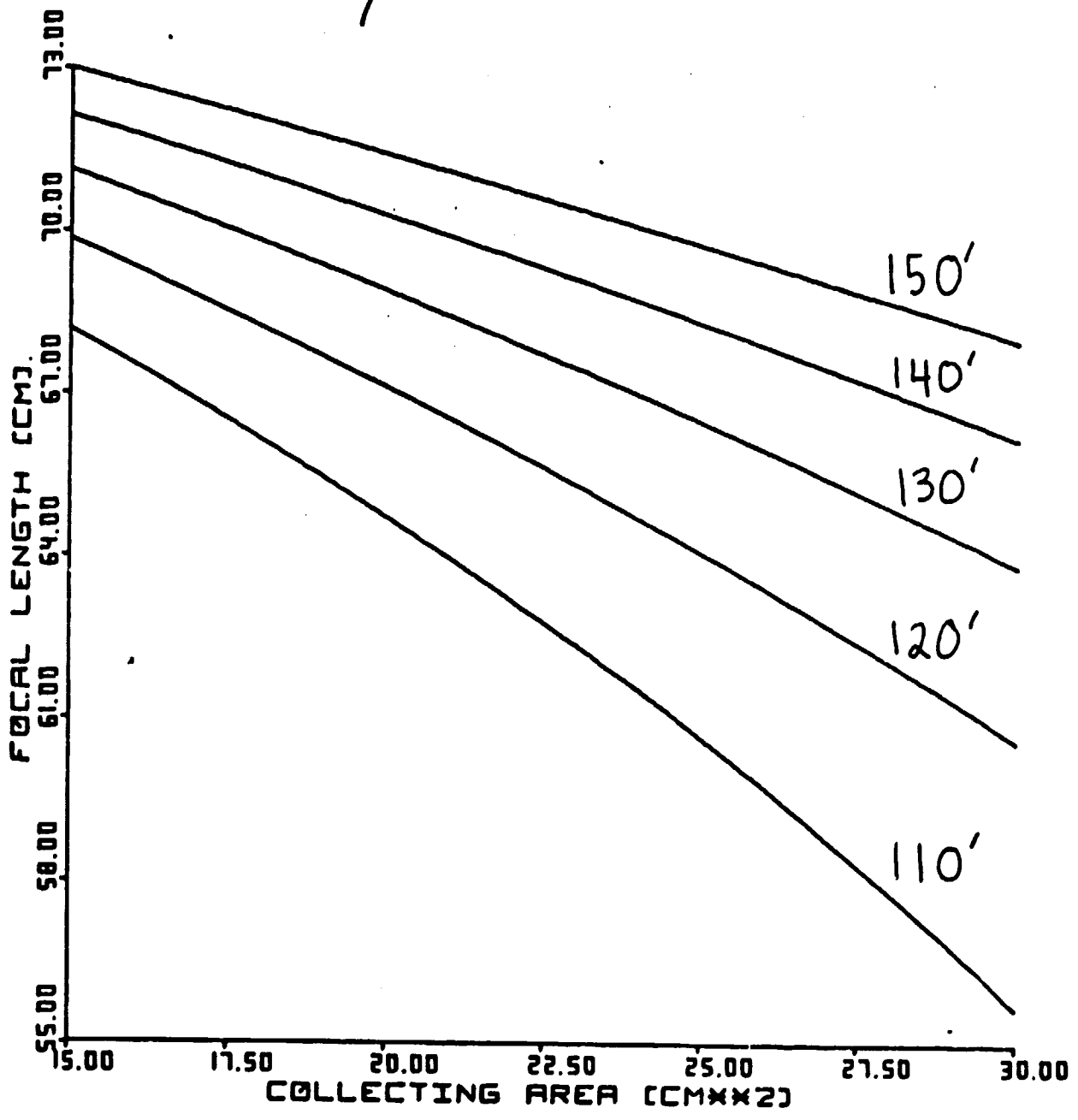


Fig. A-2